# Collision dynamics and reactions of fractional vortex molecules in coherently coupled Bose-Einstein condensates

Minoru Eto[1,2] Kazuki Ikeno,[3] and Muneto Nitta[2,4,*]

[1]*Department of Physics, Yamagata University, Kojirakawa-machi 1-4-12, Yamagata, Yamagata 990-8560, Japan*
[2]*Research and Education Center for Natural Sciences, Keio University, Hiyoshi 4-1-1, Yokohama, Kanagawa 223-8521, Japan*
[3]*Adavito Inc., Hongo-cho 4-26-12, Bunkyo-ku, Tokyo, 113-033, Japan*
[4]*Department of Physics, Keio University, Hiyoshi 4-1-1, Yokohama, Kanagawa 223-8521, Japan*

(Received 18 December 2019; accepted 30 March 2020; published 8 September 2020)

Coherently coupled two-component Bose-Einstein condensates (BEC) exhibit vortex confinement resembling quark confinement in quantum chromodynamics (QCD). Fractionally quantized vortices winding only in one of two components are attached by solitons, and they cannot stably exist alone. Possible stable states are "hadrons" either of mesonic type, i.e., molecules made of a vortex and antivortex in the same component connected by a soliton, or of baryonic type, i.e., molecules made of two vortices winding in two different components connected by a soliton. Mesonic molecules move straight with a constant velocity while baryonic molecules rotate. We numerically simulate collision dynamics of mesonic and baryonic molecules and find that the molecules swap partners in collisions in general like chemical and nuclear reactions, as well as summarizing all collisions as vortex reactions, and describe those by Feynman diagrams. We find a selection rule for final states after collisions of vortex molecules, analogous to that for collisions of hadrons in QCD.

DOI: 10.1103/PhysRevResearch.2.033373

## I. INTRODUCTION

Ultracold atomic gases are experimentally controllable systems offering setups to simulate various problems in physics [1–3]. For instance, Bose-Einstein condensates (BECs) are superfluids admitting quantized vortices, i.e., vortices carrying quantized circulations [4] known as global strings in cosmology, and nucleation of vortices and detecting real-time dynamics of them were achieved experimentally recently [5]. Among various systems, coherently coupled two-component BECs realized by the JILA group [6,7] are one interesting system for understanding high-energy physics; when each component is a different hyperfine state of the same atom, one can introduce a Rabi (Josephson) coupling between them. Then they allow vortex molecules, fractionally quantized vortices confined by solitons (linearly extended objects) [8], which are suggested to share several properties with confinement phenomena of quantum chromodynamics (QCD), a theory of the strong interaction consisting of quarks and gluons. Such fractional vortex molecules have been extensively studied theoretically [9–17], including sine-Gordon like solitons [18–21]. Moreover, such studies have been extended to three or more components [22–27] as well as spinor BECs [28]. Similarities with QCD were found by studying the dynamics of a single vortex molecule composed of two fractional vortices [14,16], for which a vortex in the first component and that in the second component are confined by a sine-Gordon soliton. If the two vortices are at an equilibrium distance, then the molecule is static. On the other hand, if they are slightly more separated or instead pulled closer together, then the molecule rotates clockwise or counterclockwise, respectively. If they are further pulled to be more separated, then the soliton connecting them is broken by creating another pair of fractional vortices, and therefore fractional vortices can never be liberated (unless the Rabi coupling is turned off). This situation resembles the confinement of quarks in QCD; the QCD vacuum is considered to be a dual superconductor [29–31], where chromoelectric fluxes are confined to color electric flux tubes due to the condensation of magnetic monopoles. Then quarks are confined by color electric flux tubes with energy linearly dependent on the distance between them.

In Ref. [16], we previously indentified fractionally quantized vortices winding in the first and second components as an up-type vortex (or u-vortex for short) and a down-type vortex (or d-vortex), respectively, borrowing the terminology from quarks in QCD. Similarly, we have called an antivortex of the first (second) component, the $\bar{\mathrm{u}}$- ($\bar{\mathrm{d}}$-) vortex. In the presence of the Rabi coupling, the elementally topological objects are composite defects of u- and d-vortices and the solitons connecting them. There are two possibilities for the soliton to select the vortices in a pair on its two endpoints: Either a vortex and an antivortex in the same component such as u and $\bar{\mathrm{u}}$ (d and $\bar{\mathrm{d}}$) or vortices in different species such as u and d ($\bar{\mathrm{u}}$ and $\bar{\mathrm{d}}$). We have called the former a mesonic vortex molecule and the latter a baryonic vortex molecule in analogy with QCD. Let us regard quantized circulations

*meto(at)sci.kj.yamagata-u.ac.jp, nitta(at)phys-h.keio.ac.jp

TABLE I. Topological winding numbers $n_1$, $n_2$, $n_S$, and $n_R$ are shown.

| | $n_1$ | $n_2$ | $n_S$ (baryon #) | $n_R$ (color charge) | $2n_R$ |
|---|---|---|---|---|---|
| u | 1 | 0 | 1/2 | 1/2 | 1 |
| d | 0 | 1 | 1/2 | −1/2 | −1 |
| ū | −1 | 0 | −1/2 | −1/2 | −1 |
| $\bar{\text{d}}$ | 0 | −1 | −1/2 | 1/2 | 1 |
| ūu | 0 | 0 | 0 | 0 | 0 |
| $\bar{\text{d}}$d | 0 | 0 | 0 | 0 | 0 |
| ūd | −1 | 1 | 0 | −1 | −2 |
| $\bar{\text{d}}$u | 1 | −1 | 0 | 1 | 2 |
| ud | 1 | 1 | 1 | 0 | 0 |
| ū$\bar{\text{d}}$ | −1 | −1 | −1 | 0 | 0 |

$n_S$ as the baryon number in QCD and the winding $n_R$ of the relative phase between the two components as the color charge. Then u- and d-vortices carrying fractional baryon-number-like quarks carry a color charge and therefore cannot exist alone. On the other hand, mesonic molecules ūu and $\bar{\text{d}}$d do not carry the baryon number like mesons, whereas baryonic molecules ud carry one baryon number, but both do not carry a color charge (color singlets) and therefore can exist stably. Table I shows a summary of possible states.

In this paper, in order to further understand the similarities between BECs and QCD, we focus on the few-body dynamics of vortex molecules, more precisely their collisions, in contrast to previous works focusing on dynamics of either single molecules [14–16] or many molecules describing vortex lattices [12] or the Berezinskii-Kosterlitz-Thouless transition [17]. Our numerical studies are twofold: the meson-meson scattering and the meson-baryon scattering. First, we investigate the meson-meson scattering of the same species (ūu-ūu). First, we simulate head-on collisions (zero impact parameter) by varying the incident angle. We show that the constituent vortices swap the partners in collisions. The recombination can be understood as a collision of the SG and anti-SG solitons, and the swapping is nothing but the pair annihilation and creation of the confining SG solitons. The simulation with the initial relative angle $\pi$ happens to show the right-angle scattering of the two mesons, which is very common among relativistic topological solitons. We then develop a useful description by employing Feynman diagrams to describe the various vortex collision events. We also study the meson-meson scatterings with nonzero impact parameter.

We then study the meson-meson scattering of the different species (ūu-$\bar{\text{d}}$d). We find that in head-on collision with zero relative angle, the scattering of the two SG solitons occurs. For head-on collisions at smaller relative angles, the incoming u and d mesons are converted into intermediate baryon and antibaryon pairs during collisions. The intermediate baryons rotate, and then they are reformed back into the mesons at the second recombination. Forming the intermediate baryonic state results in the shift of the outgoing line from the ingoing one. We also study the scattering with nonzero impact parameters in this case, too.

Next we study the meson-baryon scattering (ūu and ud) and find that the meson and baryon swap their constituent u-vortices, with the new meson leaving while the new baryon remains at slightly shifted point from the original baryon position. For scattering of a long meson into a baryon, the recombination takes place also in this case, so that a long and kink bend baryon is formed at first stage, and subsequently a long and bent molecule is unstable and soon disintegrates into a shorter meson and a shorter baryon. As a result, the final state comprises more molecules than the initial configuration, resembling what happens in real hadron collider experiments. We exaggeratedly call it a vortical hadron jet in the vortical hadron collider (VHC) experiment.

We then further discuss a connection between BEC and QCD comparing Polyakov's dual photon model in $2+1$ dimensions to the low-energy effective theory based on two-component BECs. We also point out that the so-called Okubo-Zweig-Iizuka (OZI) rule [32–34], which is a phenomenological law concerning final states of hadronic collisions found in the 1960s [35], seems to hold in vortex molecule collisions in BECs.

This paper is organized as follows. In Sec. II, we introduce our model and describe mesonic and baryonic vortex molecules. In Secs. III and IV, we study the meson-meson scattering of the same species (ūu-ūu) and of the different species (ūu-$\bar{\text{d}}$d), respectively. In Sec. V, we study the meson-baryon scatterings (ūu and ud). In Sec. VI, we give comments on a connection between BEC and QCD. Finally, Sec. VII is devoted to a summary and discussion.

## II. HADRONIC VORTEX MOLECULES

Theoretically, the dynamics of the condensates $\Psi_i$ can be described by the coupled Gross-Pitaevskii (GP) equations,

$$\left[i\hbar\frac{\partial}{\partial t}+\frac{\hbar^2}{2m}\nabla^2-\left(g_i|\Psi_i|^2+g_{12}|\Psi_{\hat{i}}|^2-\mu_i\right)\right]\Psi_i = -\hbar\omega\Psi_{\hat{i}}, \quad (i=1,2), \tag{1}$$

where we use the notation $\hat{1}=2$, $\hat{2}=1$, $g_{ij}$ represents the atom-atom coupling constants, $m$ is the mass of atom, and $\mu_i$ represents the chemical potential of each component. The first and second condensates $\Psi_{1,2}$ are coherently coupled through the Rabi (Josephson) terms with the Rabi frequency $\omega$. Experimentally, such a coherent coupling was achieved by the JILA group [7]. In the following, we assume

$$g_1=g_2\equiv g, \quad \mu_1=\mu_2\equiv\mu, \tag{2}$$

and, for simplicity, we focus on a miscible BEC ($g>g_{12}$) in which both condensates spatially coexist with

$$|\Psi_1|=|\Psi_2|=\sqrt{\frac{\mu+\hbar\omega}{g+g_{12}}}\equiv v. \tag{3}$$

If the Rabi interaction is turned off $\omega=0$, then the system has two $U(1)$ symmetries $U(1)_1\times U(2)_2$ defined by

$$U(1)_1:\ (\Psi_1,\ \Psi_2)\to(e^{i\alpha_1}\Psi_1,\Psi_2),$$
$$U(1)_2:\ (\Psi_1,\ \Psi_2)\to(\Psi_1,e^{i\alpha_2}\Psi_2). \tag{4}$$

These symmetries can also be expressed as

$$[U(1)_S\times U(1)_R]/\mathbb{Z}_2:(\Psi_1,\Psi_2)\to(e^{i\alpha}\Psi_1,e^{\pm i\alpha}\Psi_2), \tag{5}$$

where + is for $U(1)_S$ and − is for $U(1)_R$, and $\mathbb{Z}_2$ represents simultaneous rotations of $U(1)_S$ and $U(1)_R$ with angle $\alpha = \pi$ for both components, which has been introduced to remove a redundancy. When $\omega \neq 0$, the relative $U(1)_R$ is manifestly broken. Namely, the number of atoms in each individual component is not preserved, but the total number of atoms across both components is preserved.

In the following, we will numerically solve the GP equation (1). For that purpose it is convenient first to rewrite it in terms of dimensionless variables,

$$\tilde{t} = \frac{\mu}{\hbar}t, \quad \tilde{x}_i = \frac{\hbar}{\sqrt{m\mu}}x_i, \quad \tilde{\omega} = \frac{\hbar}{\mu}\omega,$$
$$\tilde{g}_{12} = \frac{g_{12}}{g}, \quad \tilde{\Psi}_i = \sqrt{\frac{g}{\mu}}\Psi_i. \tag{6}$$

Then, the GP equation can be rewritten as

$$\left[i\frac{\partial}{\partial\tilde{t}} + \frac{1}{2}\tilde{\nabla}^2 - \left(|\tilde{\Psi}_i|^2 + \tilde{g}_{12}|\tilde{\Psi}_{\bar{i}}|^2 - 1\right)\right]\tilde{\Psi}_i = -\tilde{\omega}\tilde{\Psi}_{\bar{i}}, \quad (i = 1, 2). \tag{7}$$

Thus, the essential parameters are only $\tilde{\omega}$ and $\tilde{g}_{12}$. In what follows, we will assume $\tilde{g}_{12} \neq 1$.

When $\tilde{\omega} = 0$, both the $U(1)_1 \times U(1)_2$ are spontaneously broken in the ground state. As a consequence, there are two kinds of topologically stable vortices supported by topological winding number $\pi_1(U(1)_1 \times U(1)_2) = \mathbb{Z} \times \mathbb{Z}$. A vortex associated with the first $U(1)_1$ at the origin, which we will call the u-vortex, is given by

$$\text{u-vortex}: \quad \tilde{\Psi}_1 = \tilde{f}(\tilde{r})e^{i\theta}, \quad \tilde{\Psi}_2 = \tilde{g}(\tilde{r}), \tag{8}$$

with $\tilde{r} = \sqrt{\tilde{x}_1^2 + \tilde{x}_2^2}$. Similarly, a vortex associated with the second $U(1)_2$ at the origin, which we will call the d-vortex, is given by

$$\text{d-vortex}: \quad \tilde{\Psi}_1 = \tilde{g}(\tilde{r}), \quad \tilde{\Psi}_2 = \tilde{f}(\tilde{r})e^{i\theta}. \tag{9}$$

A u-vortex becomes an anti-u-vortex (we will refer to it as a $\bar{\text{u}}$-vortex) by exchanging $\theta \to -\theta$. Similarly, a d-vortex and a $\bar{\text{d}}$-vortex are replaced by $\theta \to -\theta$. The profile functions $\tilde{f}$ and $\tilde{g}$ satisfy the following second-order ordinary differential equations:

$$\left[\frac{1}{2}\left(\frac{\partial^2}{\partial\tilde{r}^2} + \frac{1}{\tilde{r}}\frac{\partial}{\partial\tilde{r}} - \frac{1}{\tilde{r}^2}\right) - (\tilde{f}^2 + \tilde{g}_{12}\tilde{g}^2 - 1)\right]\tilde{f} = 0, \tag{10}$$

$$\left[\frac{1}{2}\left(\frac{\partial^2}{\partial\tilde{r}^2} + \frac{1}{\tilde{r}}\frac{\partial}{\partial\tilde{r}}\right) - (\tilde{g}^2 + \tilde{g}_{12}\tilde{f}^2 - 1)\right]\tilde{g} = 0. \tag{11}$$

The appropriate boundary conditions are

$$\lim_{\tilde{r}\to 0}\tilde{f} = 0, \quad \lim_{\tilde{r}\to\infty}\tilde{f} = \tilde{v}_0, \quad \lim_{\tilde{r}\to 0}\frac{\partial\tilde{g}}{\partial\tilde{r}} = 0, \quad \lim_{\tilde{r}\to\infty}\tilde{g} = \tilde{v}_0, \tag{12}$$

where we have defined

$$\tilde{v}_0 = \frac{1}{\sqrt{1 + \tilde{g}_{12}}}. \tag{13}$$

Figure 1 shows a typical numerical solution of $\tilde{f}$ and $\tilde{g}$ for $\tilde{g}_{12} = 0.5$ as an example.

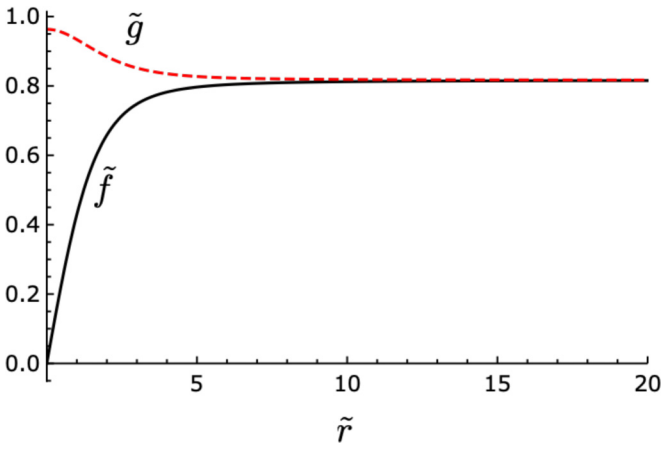


FIG. 1. The profile functions $\tilde{f}$ and $\tilde{g}$ of a u- or d-vortex for $\tilde{g}_{12} = 0.5$. The Rabi term is suppressed ($\tilde{\omega} = 0$).

It is useful to introduce the pseudospin to distinguish u- and d-vortices,

$$\boldsymbol{S} = -\frac{\vec{\Psi}^\dagger\boldsymbol{\sigma}\vec{\Psi}}{\vec{\Psi}^\dagger\vec{\Psi}}, \quad \vec{\Psi} = (\Psi_1, \Psi_2), \tag{14}$$

with the Pauli matrices $\boldsymbol{\sigma}$. $\boldsymbol{S}$ is a real three-vector satisfying $|\boldsymbol{S}| = 1$, and so it can be thought of as coordinates of an internal $S^2$ target space. The pseudospin $\boldsymbol{S}$ is transformed as a triplet **3** under the $SU(2)$ transformation $\vec{\Psi} \to U\Psi$ with $U \in SU(2)$. Note that the $SU(2)$ symmetry is the only manifest symmetry which comes from part of the GP equations, namely the gradient terms of Eq. (1). The remaining terms of Eq. (1) generally do not respect the $SU(2)$ symmetry but instead respect the subgroup $U(1)_R \subset SU(2)$. Only when $g = g_{12}$ ($\tilde{g}_{12} = 1$) together with the fulfillment of condition (2) is the system symmetry $U(1)_1 \times U(1)_2$ enhanced to $[U(1)_S \times SU(2)]/\mathbb{Z}_2$. Otherwise, the $SU(2)$ symmetry is the only approximate symmetry of the generic GP equation (1). The u- and d-vortices have $(\tilde{\Psi}_1(0,0), \tilde{\Psi}_2(0,0)) = (0, \tilde{g}(0))$ and $(\tilde{g}(0), 0)$ at their cores, so that their pseudospins are $\boldsymbol{S} = (0, 0, 1)$ (up) and $\boldsymbol{S} = (0, 0, -1)$ (down), respectively. Figure 2 shows the pseudospins of the u- and d-vortices.

When $\tilde{\omega} = 0$, the vortex number can be measured by

$$n_i = \frac{1}{2\pi}\oint_C d\theta_i = \frac{1}{2\pi}\int_0^{2\pi}\frac{d\theta_i}{d\theta}d\theta, \tag{15}$$

where $\theta_i$ is the phase of $\Psi_i$ ($\theta_i = \arg\Psi_i$) and C is a closed curve in the $x^1$-$x^2$ plane.

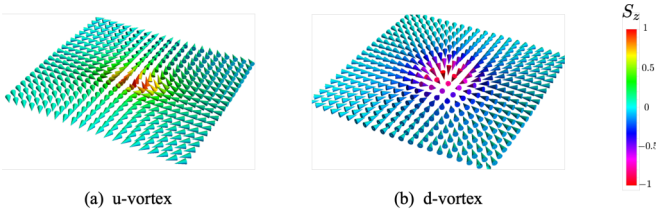


(a) u-vortex (b) d-vortex

FIG. 2. Vector plots of the pseudospin $\boldsymbol{S}(x^1, x^2)$ for the u-vortex in panel (a) and d-vortex in panel (b) (constructed from the solution given in Fig. 1) are plotted on the $x^1$-$x^2$ plane ($\tilde{x}^{1,2} \in [-5, 5]$). The colors of arrows represent $S_z$. The Rabi frequency is set to $\tilde{\omega} = 0$.

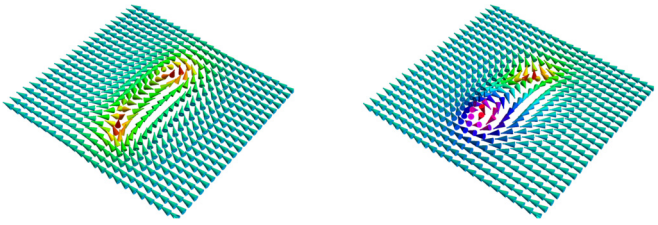

(a) mesonic molecule $\bar{u}u$ (b) baryonic molecule ud

FIG. 3. Vector plots of the pseudospin $\boldsymbol{S}(x^1, x^2)$ for the $\bar{u}u$ and ud are plotted on the $x^1$-$x^2$ plane. The plot region of panel (a) is $\tilde{x}^1 \in [-10, 10]$ and $\tilde{x}^2 \in [40, 60]$ and that for panel (b) is $\tilde{x}^1 \in [-10, 10]$ and $\tilde{x}^2 \in [-10, 10]$. The color map is the same as the one in Fig. 2. The Rabi frequency is set to be $\tilde{\omega} = 0.05$.

When $\tilde{\omega} \neq 0$, neither the u- nor the d-vortex exists alone since $U(1)_R$ is manifestly broken. The winding numbers $n_1$ and $n_2$ are no longer good topological numbers. The Rabi term effectively works as a sine-Gordon– (SG) type potential,

$$V_{\text{Rabi}} = -2\hbar\omega v^2 \cos(\theta_1 - \theta_2), \tag{16}$$

where we have set $\psi_i = ve^{i\theta_i}$. Due to this, the u-vortex given in Eq. (8) with $(\theta_1, \theta_2) = (\theta, 0)$ is inevitably attached to a SG soliton at $\theta = \pi$. For the same reason, the d-vortex given in Eq. (9), the $\bar{u}$-vortex and $\bar{d}$-vortex are also attached to a SG or an anti-SG soliton. Under the nonzero $\tilde{\omega}$, it turns out that the following are more useful than $n_1$ and $n_2$:

$$n_S = \frac{1}{2\pi}\oint_C d\theta_S = \frac{1}{2\pi}\int_0^{2\pi}\frac{1}{2}\left(\frac{d\theta_1}{d\theta} + \frac{d\theta_2}{d\theta}\right)d\theta = \frac{n_1 + n_2}{2}, \tag{17}$$

$$n_R = \frac{1}{2\pi}\oint_C d\theta_R = \frac{1}{2\pi}\int_0^{2\pi}\frac{1}{2}\left(\frac{d\theta_1}{d\theta} - \frac{d\theta_2}{d\theta}\right)d\theta = \frac{n_1 - n_2}{2}, \tag{18}$$

with $\theta_S = (\theta_1 + \theta_2)/2$ and $\theta_R = (\theta_1 - \theta_2)/2$. Here $n_S$ and $n_R$ are topological invariants taking values in half integers when $\tilde{\omega} = 0$. Once we turn on $\tilde{\omega} \neq 0$, $n_R$ is no longer a topological number. Though $n_R$ is not preserved, it has another physical meaning: $2n_R$ corresponds to the total SG soliton number across the curve C. For a single u-vortex, we have $2n_R = 1$ for any C which encloses it. We summarize $n_1$, $n_2$, $n_S$, and $n_R$ in Table I. From this, we see that u- and $\bar{d}$-vortices are attached by a SG soliton while $\bar{u}$- and d-vortices are attached by an anti-SG soliton.

However, this is only a static picture. Since a semi-infinitely long soliton costs infinite energy, it is dynamically unstable and disintegrates into shorter solitons. A finite soliton is terminated by two vortices, namely it forms a vortex molecule with the SG soliton bounding two vortices. We can figure out all possible types of molecules by seeing $n_R$. Since a vortex molecule is finite configuration, the corresponding $n_R$ for a sufficiently large C enclosing it must be zero. Therefore, there exist four kinds of molecules, $\bar{u}u$, $\bar{d}d$, ud, and $\bar{u}\bar{d}$. We plot the pseudospins of $\bar{u}u$ and ud molecules in Fig. 3.

This phenomenon resembles quark confinement in QCD. The quarks are elementary particles in nature, but they are confined in the form of hadrons and we cannot remove individual quarks out from a hadron. Quarks in QCD resemble our "elementary" u- and d-vortices in two-component BECs. One might envisage that the isospin of up- and down-quarks is a natural counterpart of the pseudospin. Furthermore, as is well known, a hadron consists of several quarks whose total color charge is zero [singlet of $SU(3)$ color group]. Now, it is natural to relate the $U(1)_R$ winding number $n_R$ of the "elementary" vortices (u, d, $\bar{u}$, $\bar{d}$) with the color charge of the quarks. Namely, a hadron in a two component BEC is a singlet state by means of $n_R = 0$. Moreover, we can also relate the $U(1)_S$ winding number $n_S$ of the elementary vortices (u- and d-vortices have $1/2$, and $\bar{u}$- and $\bar{d}$-vortices have $-1/2$, winding number) with the baryon number of the quarks (a quark has $1/3$ and an antiquark has $-1/3$ baryon number). Hadrons with baryon number $+1(-1)$ are called baryons (antibaryons), and those with no baryon number are called mesons in QCD. Borrowing the terminology from QCD, we may associate a ud-vortex molecule to a baryon since it has $n_S = 1$ and the $\bar{u}\bar{d}$-vortex molecule to an antibaryon with $n_S = -1$. Similarly, we term the $\bar{u}u$ molecule a u meson while the $\bar{d}d$ molecule a d meson because they have $n_S = 0$. Of course, though this analogy between two component BECs and QCD is limited, it is very useful. For example, the $\bar{u}d$ meson does not exist in the BEC system because its $U(1)_R$ winding number is not zero, see Table I. We will give more details of a relation between QCD and BECs in Sec. VI.

Let us next mention the dynamics of the mesonic and baryonic vortex molecules. A meson propagates with an almost constant velocity toward the direction perpendicular to the molecule. This motion can be understood by a Magnus force between the vortex and the antivortex within the meson. For a long meson the attractive force is dominated by the SG soliton and therefore the moving speed is almost constant. On the other hand, the attractive force originates in an intervortex force that dominates for a shorter meson. Therefore, the shorter meson moves faster. However, these observations are valid only for a meson with reasonable length. If the meson is too short, then it soon decays. If the meson is too long, then it soon disintegrates [16]. We show a typical motion of a u meson in Fig. 4. We initially place a meson whose length is about 10 in terms of the dimensionless coordinate $\tilde{x}_i$. We put the meson at $(\tilde{x}_1, \tilde{x}_2) = (0, 50)$ at $\tilde{t} = 0$ (the pseudospin of the initial state is given in the left panel of Fig. 3). It moves downward and passes through the origin around $\tilde{t} = 100$. During the simulation, the soliton periodically bends forward and backward, and the distance between the u and $\bar{u}$ periodically gets shorter and longer.

On the other hand, a baryon moves very differently. It does not propagate linearly but instead rotates with an almost constant angular speed [14,16]. When the baryon is longer, the motion is dominated by an attractive force due to the soliton. On the other hand, when the baryon is shorter, the soliton tension and the intervortex force compete. When $g_{12} > 0$, the intervortex force is repulsive [36]. The shorter the baryon is, the stronger the intervortex force is. On the contrary, when the baryon is too short, the soliton tension becomes negligible. Therefore, the rotating speed of the baryon for $g_{12} > 0$

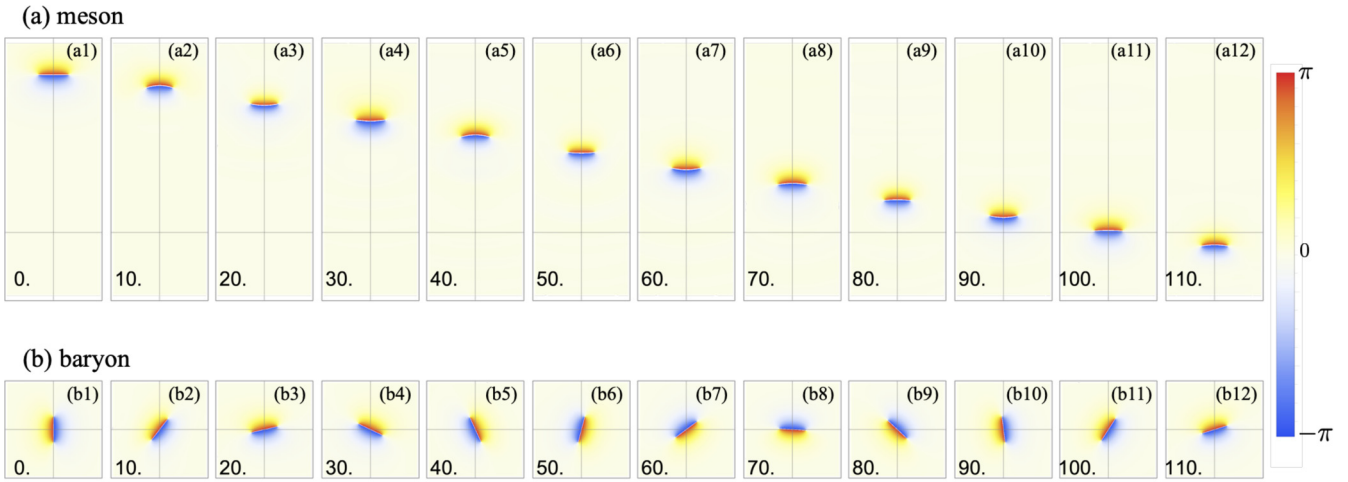


FIG. 4. The upper panels (a1)–(a12) show the motion of a single u meson, and the lower panels (b1)–(b12) show the motion of a baryon. We choose $\tilde{g}_{12} = 0.5$ and $\tilde{\omega} = 0.05$. The color corresponds to $\arg(\Psi_1) - \arg(\Psi_2)$. The red corresponds to $\arg(\Psi_1) - \arg(\Psi_2) = \pi$ while the blue corresponds to $\arg(\Psi_1) - \arg(\Psi_2) = -\pi$. The upper panel (the horizontal region is $\tilde{x}_1 \in [-15, 15]$ and the vertical region is $\tilde{x}_2 \in [-20, 60]$): We place a single $\bar{\text{u}}$-vortex at $(\tilde{x}_1, \tilde{x}_2) = (-5, 50)$ and u-vortex at $(\tilde{x}_1, \tilde{x}_2) = (5, 50)$ at $\tilde{t} = 0$ in the leftmost figure. The lower panel (the horizontal region is $\tilde{x}_1 \in [-15, 15]$ and the vertical region is $\tilde{x}_2 \in [-15, 15]$): We put u-vortex at $(\tilde{x}_1, \tilde{x}_2) = (0, 4)$ and d-vortex at $(\tilde{x}_1, \tilde{x}_2) = (0, -4)$ at $\tilde{t} = 0$. The motion of the molecule are shown, with snapshots at time intervals of $\delta\tilde{t} = 10$.

becomes gradually smaller and it vanishes at an equilibrium. For the baryon with $g_{12} < 0$, both the intervortex interaction and soliton tension give attractive forces [36] so that such an equilibrium does not exist. Similarly to the meson, very long baryons quickly disintegrate. However, the baryon never vanishes since the $U(1)_S$ winding number is topological. Figure 4 shows a typical rotating baryon. We initially place a baryon with length about 8 in the dimensionless units at the origin at $\tilde{t} = 0$ (the pseudospin of the initial state is given in the right panel of Fig. 3). It rotates clockwise and returns to the original angle around $\tilde{t} = 90$. Similarly to mesons, it slightly vibrates during the rotation. Baryons shorter than equilibrium distance rotate counterclockwise.

Before closing this section, let us mention that there are significant differences between relativistic and nonrelativistic dynamics of vortices. Both the linear propagation of the mesonic molecule and the rotation of the baryonic molecule are specific to the nonrelativistic system. Due to these characteristic motions, molecules are quasistable. On the contrary, in relativistic systems two vortices separate (close) when the inter vortex force is repulsive (attractive), so that no stable molecules can in general exist. In what follows, we will make use of these nonrelativistic properties and numerically simulate the scattering of mesonic and baryonic molecules in two-component BECs as a vortical hadron collider.[1]

Here one comment is in order. Vortex dynamics in two-component BECs in the absence of the Rabi interaction was studied in Ref. [38,39], in which case fractional vortices are liberated. Even in such a case, the dynamics can be quite nontrivial; however, it is beyond the scope of the present paper.

[1]The movies of our numerical simulations studied below are available as the Supplemental Material [37].

## III. MESON-MESON SCATTERING: THE CASE OF ūu-ūu

### A. ūu-ūu head-on collision

Let us begin with the most elementary process, namely head-on collision of two mesons of the same species. Since we have concentrated on the symmetric model under replacement $\Psi_1$ and $\Psi_2$, we can choose the u mesons without loss of generality. We prepare an initial configuration as follows. First, we create a configuration $(\Psi_1^{(1)}, \Psi_2^{(1)})$ for the u meson $(\bar{\text{u}}_1\text{u}_1)$ corresponding to the one given in the leftmost panel of the first row in Fig. 4. Similarly, we prepare another configuration $(\Psi_1^{(2)}, \Psi_2^{(2)})$ for the u meson $(\bar{\text{u}}_2\text{u}_2)$ by rotating the $\bar{\text{u}}_1\text{u}_1$ by 180° around the origin. Then we superpose these two configurations à la the Abrikosov as

$$\Psi_i^{(\text{ini})} = \frac{1}{v}\Psi_i^{(1)}\Psi_i^{(2)}, \quad (i = 1, 2). \tag{19}$$

In this way, we have the initial configuration which has two incoming mesons $\bar{\text{u}}_1\text{u}_1$ at $(\tilde{x}_1, \tilde{x}_2) = (0, 50)$ [precisely speaking, we put a u-vortex at $(\tilde{x}_1, \tilde{x}_2) = (5, 50)$ and a $\bar{\text{u}}$-vortex at $(\tilde{x}_1, \tilde{x}_2) = (-5, 50)$] and the $\bar{\text{u}}_2\text{u}_2$ and $(\tilde{x}_1, \tilde{x}_2) = (0, -50)$ [we put a u-vortex at $(\tilde{x}_1, \tilde{x}_2) = (-5, -50)$ and a $\bar{\text{u}}$-vortex at $(\tilde{x}_1, \tilde{x}_2) = (5, -50)$]. With the initial configuration at hand, next we numerically integrate the Gross-Pitaevskii equations. The result is shown in Figs. 5 and 6.

Up to slightly before the moment of the collision ($\tilde{t} \lesssim 100$), each meson moves straight toward the origin as if the other meson does not exist. However, an interesting vortical reaction occurs during the collision. It is a recombination of the SG solitons binding the constituent vortices $\bar{\text{u}}$ and u. Before the collision, $\bar{\text{u}}_1\text{u}_1$ and $\bar{\text{u}}_2\text{u}_2$ are well separated, and the SG solitons bridge $\bar{\text{u}}_1$ and $\text{u}_1$ and also $\bar{\text{u}}_2$ and $\text{u}_2$, respectively. As can be seen in Fig. 6, $\bar{\text{u}}_1$ and $\text{u}_2$ ($\text{u}_1$ and $\bar{\text{u}}_2$) collide head on, so that two distances between $\bar{\text{u}}_1$ and $\text{u}_1$ and then $\bar{\text{u}}_1$ and $\text{u}_2$ become comparable about the moment of the collision. Then the SG solitons reconnect different pairs of $\bar{\text{u}}$ and u from the

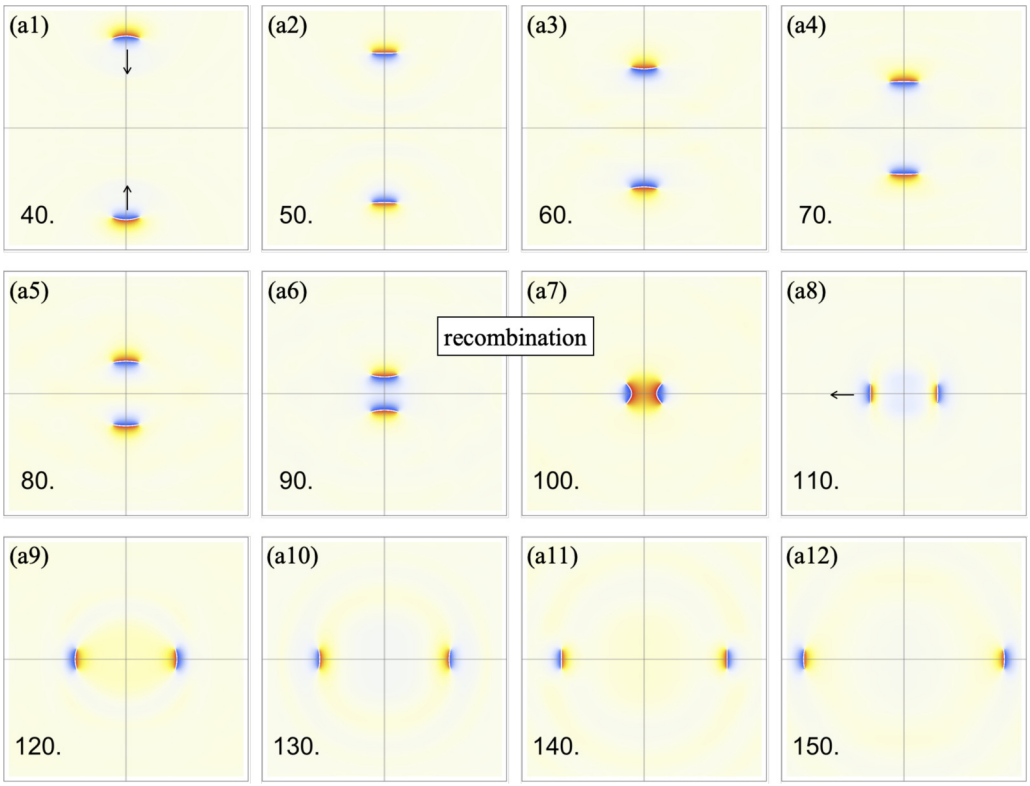


FIG. 5. Two u mesons scattering: Color density plots of the relative phase $\arg(\Psi_1) - \arg(\Psi_2)$. We initially ($\tilde{t} = 0$) set the same u meson ($\bar{u}_1 u_1$) at $(\tilde{x}_1, \tilde{x}_2) = (0, 50)$ as the one given in the leftmost panel of the upper line of Fig. 4 and the same u meson ($\bar{u}_2 u_2$) but rotated by 180° at $(\tilde{x}_1, \tilde{x}_2) = (0, -50)$. They propagate linearly with almost constant speed and collide around the origin. During the collision, the sine-Gordon (SG) solitons partially reconnect and the recombination takes place. As a consequence, the u mesons in the head-on collision scatter through a right angle. We show the snapshots from $\tilde{t} = 40$ (a1) to 150 (a12) with an interval $\delta\tilde{t} = 10$, and the plot region is $\tilde{x}_1 \in [-40, 40]$ (horizontal) and $\tilde{x}_2 \in [-40, 40]$ (vertical).

initial pairs. The new SG solitons are vertical, so that the new outgoing mesons fly along the $x^1$ axis. Namely, the u mesons in the head-on collision scatter through a right angle as a consequence of the recombination. We may describe this process as follows:

$$\bar{u}_1 u_1 + \bar{u}_2 u_2 \to \bar{u}_1 u_2 + \bar{u}_2 u_1. \tag{20}$$

Note that the subscripts (1 and 2) are introduced just for our convenience; the $u_1$- and $u_2$-vortices are the same vortices, so they are indistinguishable. In analogy with chemical and nuclear reactions, we call processes concerning vortex molecules such as Eq. (20) "vortical reactions."

Note also that the right-angle scattering of two topological solitons are common in relativistic field theories, such as with magnetic monopoles or vortices. However, the right-angle scattering is usually observed in the collisions of two solitons with the same topological charges. The right-angle scattering here is very different since mesons have zero topological charge and it occurs as a consequence of the recombination.

Let us observe the recombination phenomena more carefully. Figure 7 shows zoomed snapshots at $\tilde{t} = 95, 97.5, 100, 102.5$. We should pay attention to the orientation of the SG solitons. Looking at the leftmost panel at $\tilde{t} = 95$ of Fig. 7 from the top to the bottom along the $\tilde{x}^2$-(vertical) axis, the color first changes from red to blue, representing the upper SG soliton, and then it changes back from blue to red, representing the lower SG soliton. The deepest red region corresponds to $\theta_1 - \theta_2 = \pi$ while the deepest bluish region corresponds to $\theta_1 - \theta_2 = -\pi$. Thus, when we focus on the SG solitons, the head-on collision of the two u mesons is nothing but a scattering of the SG and anti-SG solitons. As can be seen in the panel at $\tilde{t} = 97.5$ in Fig. 7, the SG soliton and anti-SG soliton increasingly bend especially around their centers due to an attractive force so that they collide before the u- and $\bar{u}$-vortices at the edges of the SG solitons do. Then their tips annihilate each other, and they proceed to complete the recombination process; see transformation from $\tilde{t} = 97.5$ to $\tilde{t} = 100$ shown in Fig. 7. The annihilation of the SG soliton and antisolitons can be clearly seen in Fig. 8 where we plot the relative phase $\theta_1 - \theta_2$ on the $\tilde{x}^2$ axis by the blue curve. The SG soliton corresponds to the jump $\pi \to -\pi$ from left to right of the horizontal axis (the $\tilde{x}^2$ axis) while the anti-SG soliton corresponds to the opposite jump from $-\pi \to \pi$. They collide and annihilate about $\tilde{t} = 100\sim110$. To be complete, let us also look at the relative phase along the $\tilde{x}^1$ axis. It is also plotted in Fig. 8 by the red broken curve. The horizontal axis corresponds to the $\tilde{x}^1$ axis for the red broken curves. Before the collision, no SG solitons exist along the $\tilde{x}^1$ axis. However, as the SG and anti-SG solitons along the $\tilde{x}^2$ axis annihilate, a new pair of SG and anti-SG solitons on the $\tilde{x}^1$ axis are created. Hence, we find that the recombination phenomenon is taken over by the pair annihilation and creation of the SG solitons.

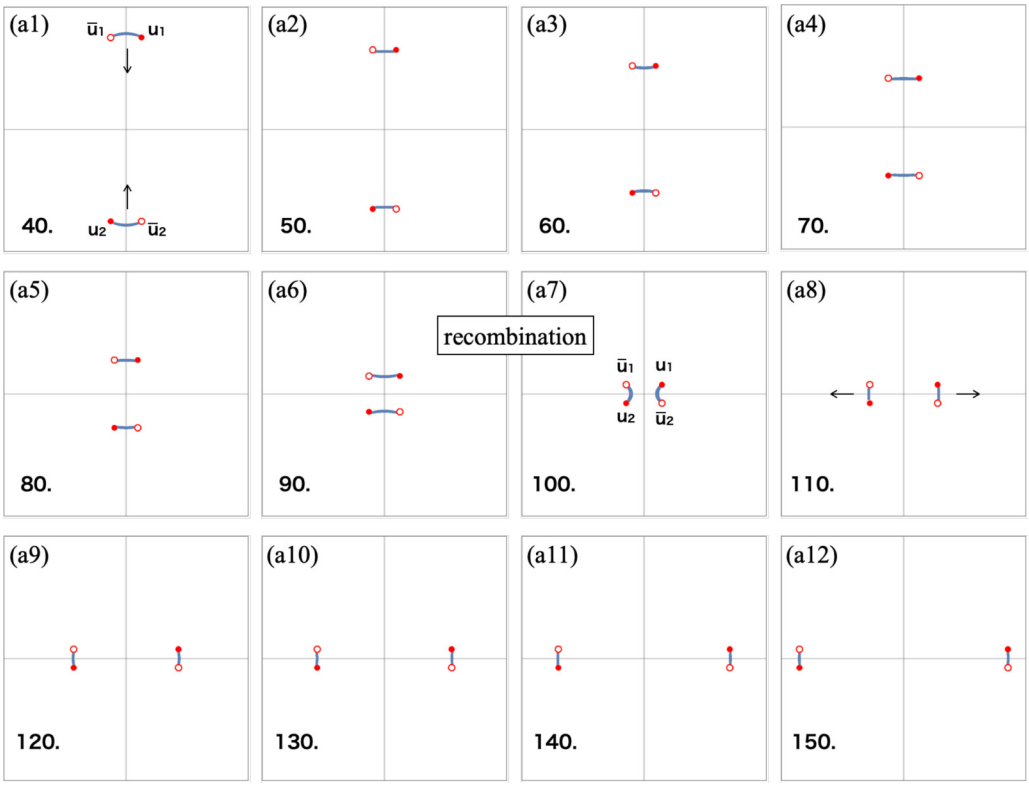


FIG. 6. A simplified plot of the u mesons scattering shown in Fig. 5. We put painted red disks (unpainted red circle) at the points corresponding to the u (ū)-vortex centers. Gray regions bridging the u and ū-vortices show the SG solitons. The gray regions are those where the relative phases take the values within $3 \leqslant |\arg(\Psi_1) - \arg(\Psi_2)| \leqslant \pi$, which are numerically obtained from Fig. 5. It is easier to understand the vortex and antivortex in this representation than Fig. 5.

### B. ūu-ūu scattering at $\pi/8$ angle

Let us next study u meson scattering similar to that in Sec. III A, but this time the upper and lower mesons are rotated by $-\pi/8$ and $\pi/8$ from those in Fig. 5. One can see the scattering behavior of the mesons in Figs. 9 and 10. Indeed, it follows qualitatively in a similar way as in the previous case. The mesons propagate linearly with almost constant speed until they are close by, and then a recombination takes place during the collision. Due to the tilts of incoming mesons,

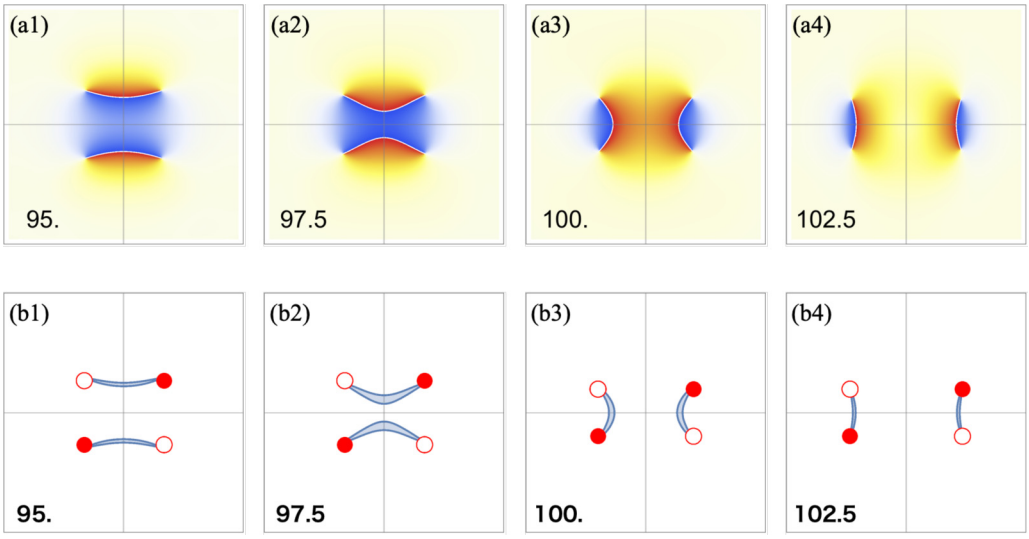


FIG. 7. Zoomed snapshots for the horizontal region $\tilde{x}_1 \in [-15, 15]$ and the vertical region $\tilde{x}_2 \in [-15, 15]$ at $\tilde{t} = 95, 97.5, 100, 102.5$ for the u meson scattering given in Figs. 5 and 6. The horizontal SG soliton incoming from the top and the antisoliton from the bottom gradually bend as they approach each other, and they partially annihilate at the tips and reconnect to form the vertical SG solitons.

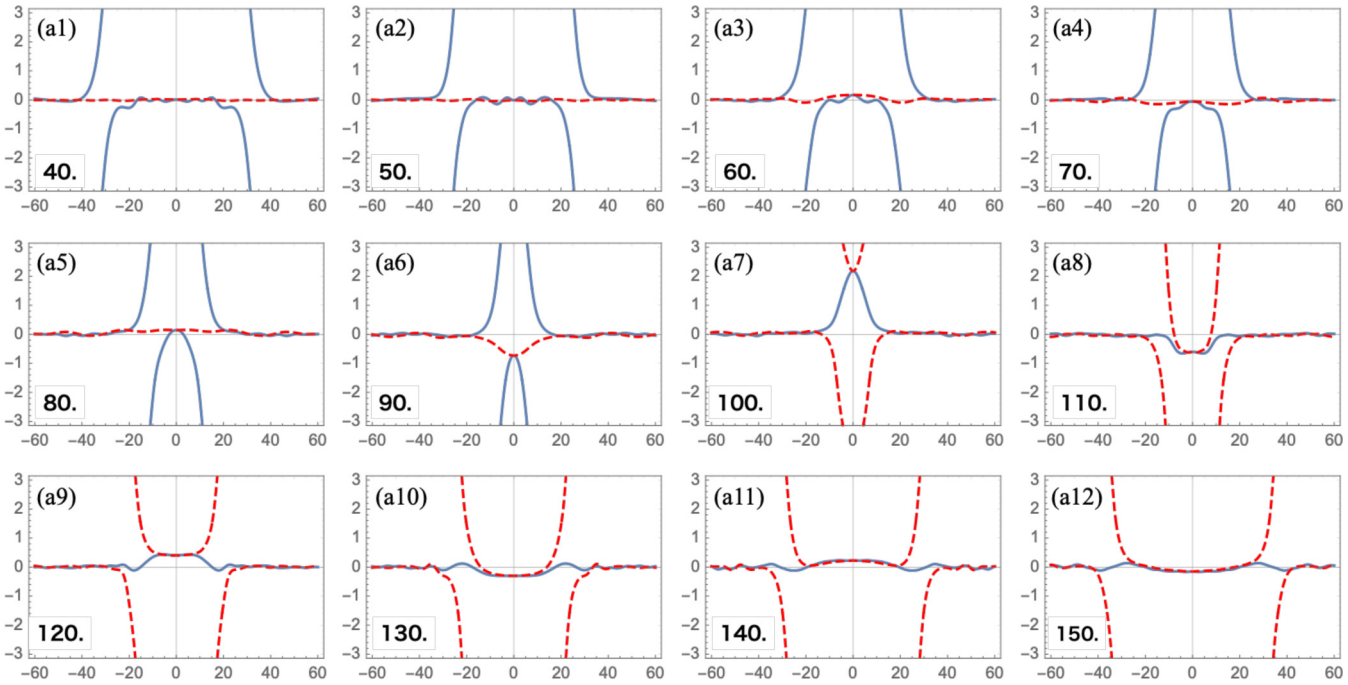


FIG. 8. The phase plots corresponding to the u meson collision in Fig. 5. The solid blue curves show the relative phase $\arg(\Psi_1) - \arg(\Psi_2)$ along the $\tilde{x}_2$ axis of Fig. 5. The SG soliton coming from the right-hand side and the anti-SG soliton coming from the left-hand side collide and annihilate. Similarly, the broken red curves show $\arg(\Psi_1) - \arg(\Psi_2)$ along the $\tilde{x}_1$ axis of Fig. 5. The SG and anti-SG solitons are pairwisely created around the moment of collision.

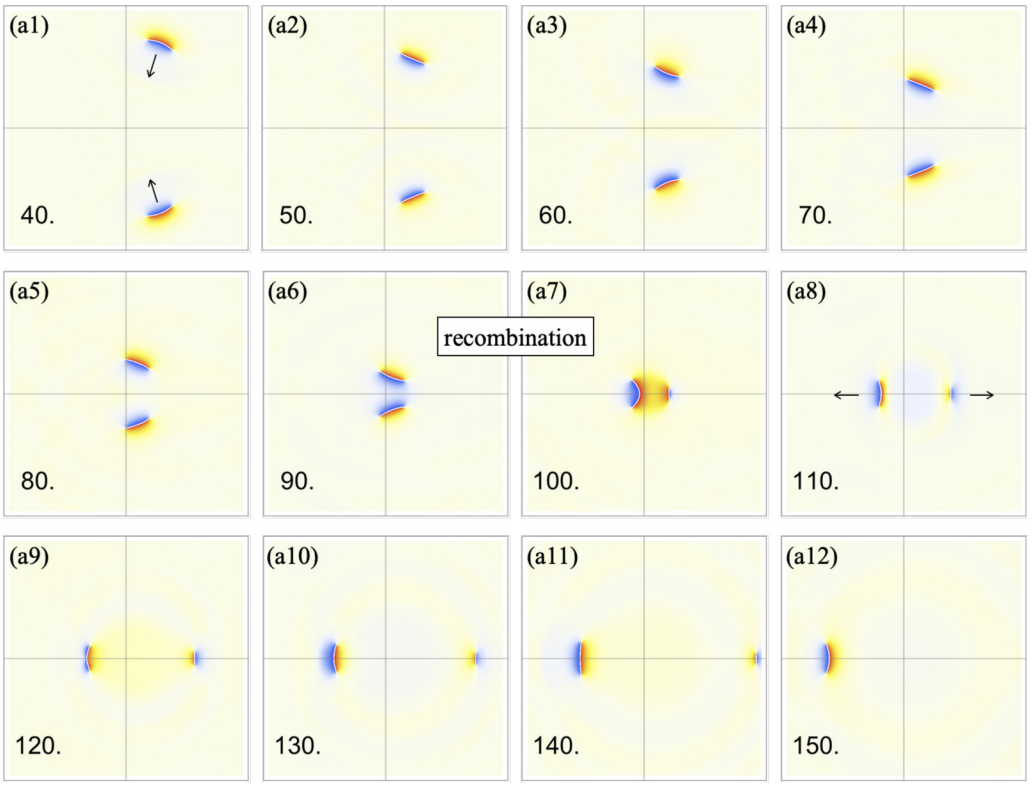


FIG. 9. Two slightly tilted u mesons scattering: Color density plots of the relative phase $\arg(\Psi_1) - \arg(\Psi_2)$. We initially ($\tilde{t} = 0$) set the u meson $(\bar{u}_1 u_1)$ at $(\tilde{x}_1, \tilde{x}_2) = (50 \sin \pi/8, 50 \cos \pi/8)$ and the other u meson $(\bar{u}_2 u_2)$ at $(\tilde{x}_1, \tilde{x}_2) = (50 \sin \pi/8, -50 \cos \pi/8)$. We only show the snapshots from $\tilde{t} = 40$ to 150 with interval $\delta\tilde{t} = 10$, and the plot region is $\tilde{x}_1 \in [-40, 40]$ (horizontal) and $\tilde{x}_2 \in [-40, 40]$ (horizontal).

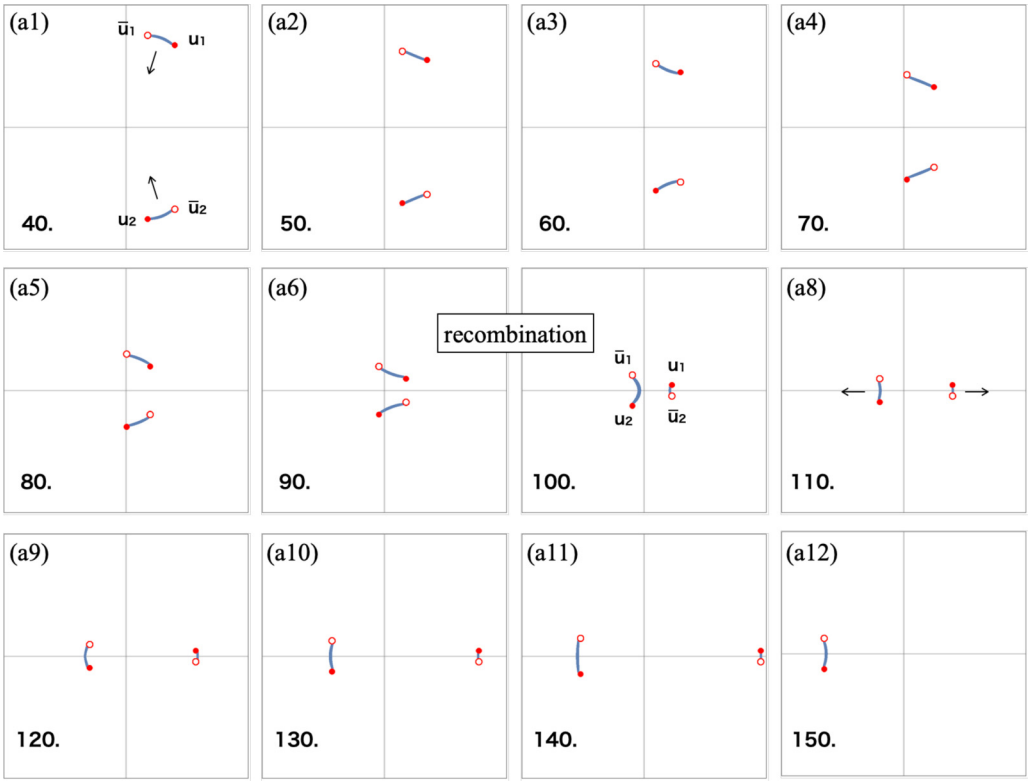


FIG. 10. A simplified plot of the u mesons scattering shown in Fig. 9. For details, see the caption of Fig. 6.

newly formed mesons are in different sizes and scatter off toward the left and right directions as the previous case. The asymmetry can also be seen in the speeds of the out-going mesons. The meson $\bar{u}_1 u_2$ moves faster than the meson $\bar{u}_2 u_1$ as shown in Fig. 10. This is because the former is shorter than the latter. Figure 11 shows zoomed snapshots at $\tilde{t} = 92.5, 95, 97.5, 100$, in which we again observe that a partial annihilation of the SG and anti-SG solitons leads to the recombination. Compared to the previous case, the bend of the SG solitons are smaller, because the bending points are

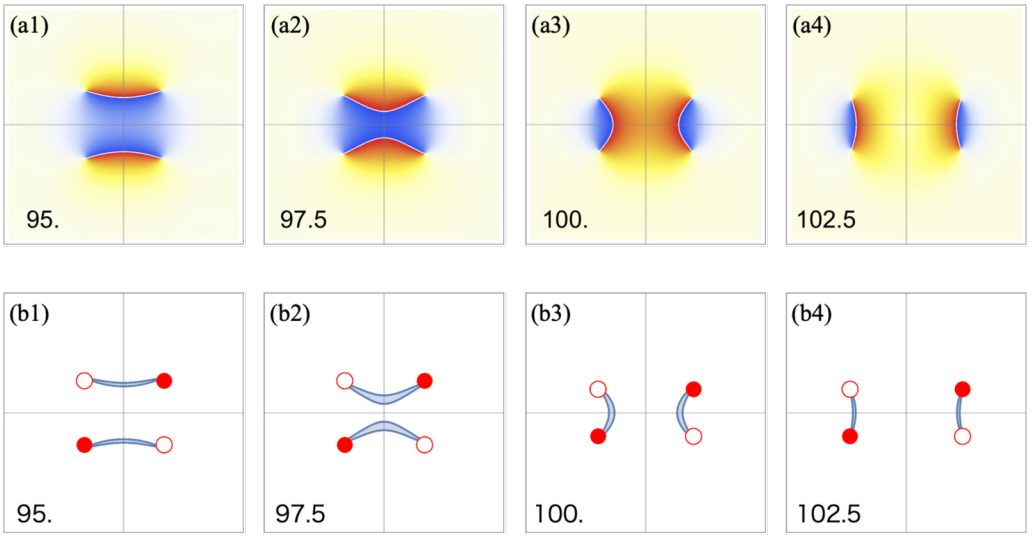


FIG. 11. Zoomed snapshots for the horizontal region $\tilde{x}_1 \in [-15, 15]$ and the vertical region $\tilde{x}_2 \in [-15, 15]$ at $\tilde{t} = 92.5, 95, 97.5, 100$ for the u meson scattering given in Figs. 9 and 10. The points where the incoming SG solitons bend steeply are not the centers. The incoming SG solitons partially annihilate around the steepest bending point and reconnect to form vertical SG solitons.

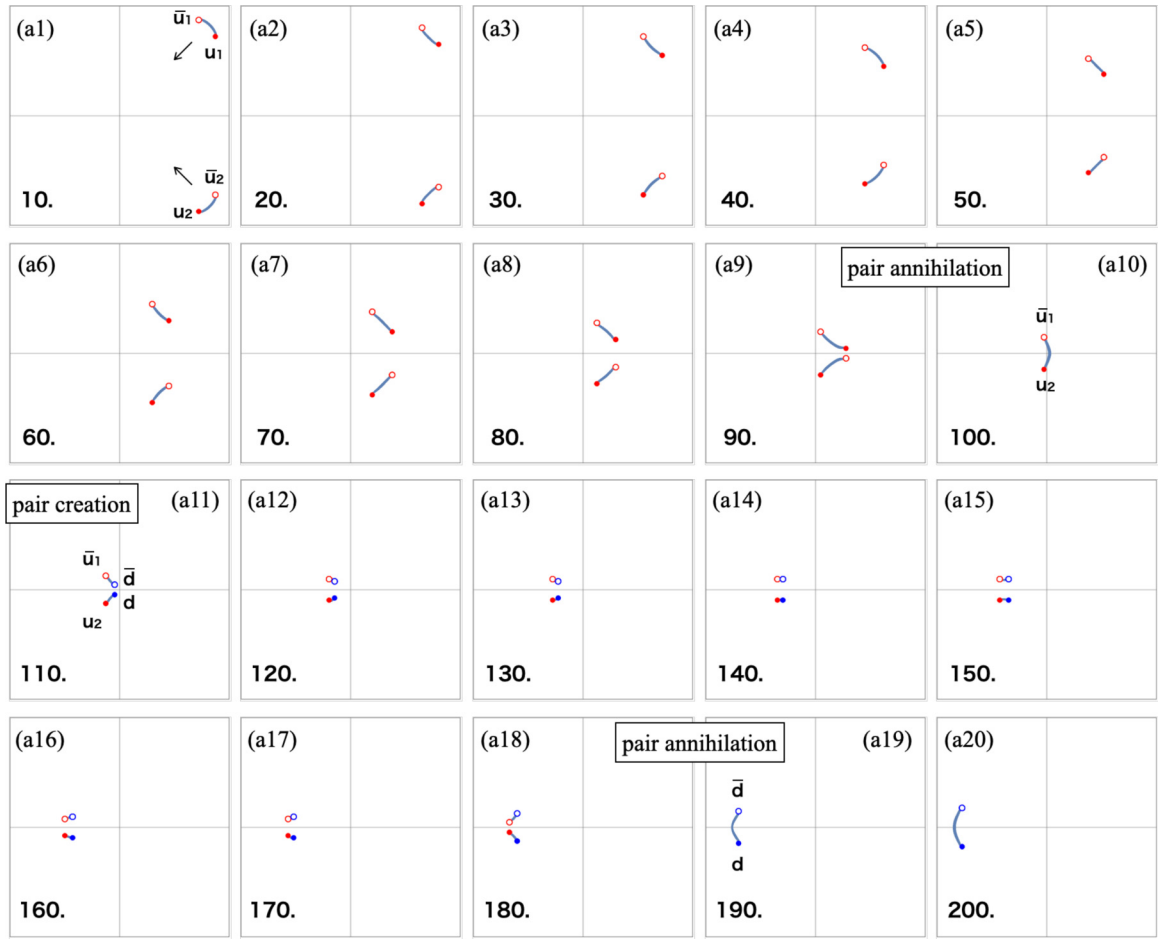


FIG. 12. Two tilted u meson scattering with $\pi/4$ angle: We initially ($\tilde{t} = 0$) place one u meson ($\bar{u}_1 u_1$) at $(\tilde{x}_1, \tilde{x}_2) = (50 \sin \pi/4, 50 \cos \pi/4)$ and the other u meson ($\bar{u}_2 u_2$) at $(\tilde{x}_1, \tilde{x}_2) = (50 \sin \pi/4, -50 \cos \pi/4)$. We only show the snapshots from $\tilde{t} = 10$ to 200 with interval $\delta\tilde{t} = 10$, and the plot region is $\tilde{x}_1 \in [-40, 40]$ (horizontal) and $\tilde{x}_2 \in [-40, 40]$ (vertical).

not at the center and are instead shifted toward the edges of the $u_1$ and $\bar{u}_2$.

### C. ūu-ūu scattering at $\pi/4$ angle

Let us attempt to simulate one more u meson scattering experiment by rotating further the incoming mesons by $\pi/4$. As expected, the motion of the mesons before the collision is almost unchanged from the previous two cases, see Fig. 12. On the contrary, the states after the collision are distinctive. First, we only observe one meson $\bar{u}_1 u_2$ after the collision. Looking at the moment of the collision in more detail, the very short $\bar{u}_2 u_1$ is created but it is soon annihilated, see Fig. 13. This occurs because the relative angle of the incoming mesons is too large. If we further rotate the initial mesons, then there is not enough time for the SG solitons to bend in order to be annihilated. Then the constituent vortices, $u_1$ and $\bar{u}_2$, are annihilated and the two SG solitons join to form a long $\bar{u}_1 u_2$ meson.

After the collision, the long meson $\bar{u}_1 u_2$ runs toward the left but such a long meson is unstable. As can be seen in Fig. 13, it soon breaks up into two pieces, the baryon ($u_2 d$) and the antibaryon ($\bar{u}_1 \bar{d}$), by creating d- and $\bar{d}$-vortices at the center of the long SG soliton. It is notable that this process is specific to two-component BECs and it has not been observed in scalar BEC systems. The baryon $u_2 d$ spins clockwise, whereas the antibaryon spins counterclockwise; see the panels with $\tilde{t} =$ 120-180 of Fig. 12. At the same time, the pair of baryon and antibaryon behave as a pair of an integer vortex and an anti-integer vortex. Thus, the baryon and antibaryon move parallel toward the left direction. After a while, the baryon and antibaryon join to form a meson $\bar{d}d$ with $\bar{u}_1$ and $u_2$ being annihilated.

Thus the corresponding reaction process can be summarized as

$$\bar{u}_1 u_1 + \bar{u}_2 u_2 \to \bar{u}_1 u_2 \to u_2 d + \bar{u}_1 \bar{d} \to \bar{d} d. \tag{21}$$

Note that the baryon number is preserved to be zero throughout the reaction.

### D. Interaction vertices and Feynman diagrams

Let us summarize the two u meson head-on scattering events described above. We found that the scattering sensitively depends on the collision angle which is direct evidence for a meson to have a substructure. We have shown three examples of the head-on collisions with relative angle $\pi$ in Fig. 6, $3\pi/4$ in Fig. 10, and $\pi/2$ in Fig. 12. An overview of the scatterings is shown in Fig. 14.

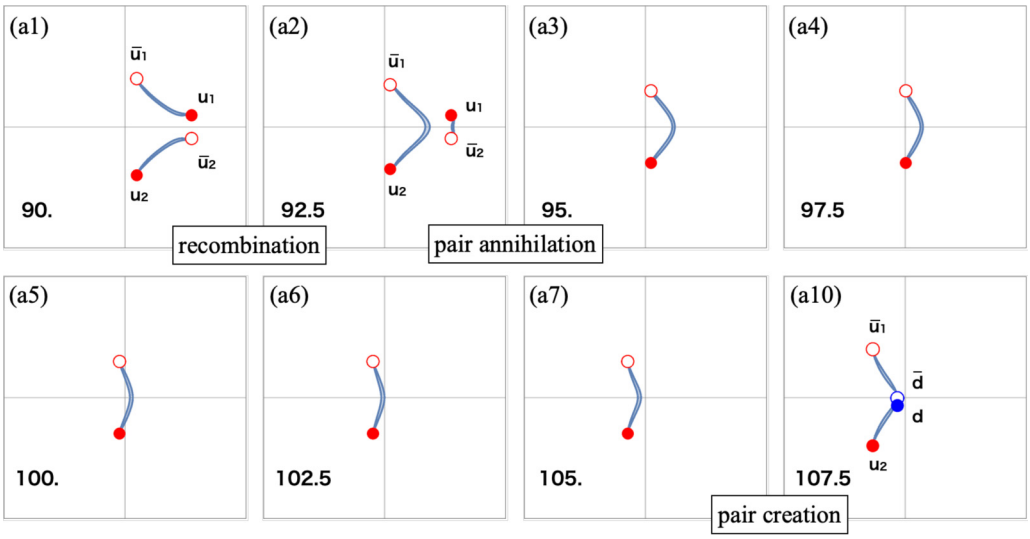


FIG. 13. Zoomed snapshots for the horizontal region $\tilde{x}_1 \in [-15, 15]$ and the vertical region $\tilde{x}_2 \in [-15, 15]$ at $\tilde{t} = 90, 92.5, 95, 97.5, 100, 102.5, 105, 107.5$ for the u meson scattering given in Figs. 12. The recombination, the pair annihilation of $\bar{u}u$, and the pair creation of $\bar{d}d$ occur in order.

Here we describe these results from a particle physics point of view. We first deal with the process given in Fig. 14(a), whose vortical reaction is given in Eq. (20). The two incoming u mesons scatter into the two outgoing u mesons. We interpret this process as an elementary interaction among mesons. Namely, this yields a meson-meson-meson-meson vertex. In order to emphasize this viewpoint, let us give a three-dimensional (3D) spacetime (two spatial and one temporal) diagram given in Fig. 15(a). It corresponds to the scattering experiment of Fig. 14(a), consisting of the world lines of the constituent vortices together with the world sheet of the SG solitons. The 3D diagram can be further simplified as in Fig. 15(a). It is a 2D diagram and resembles the so-called twig diagram (a sort of Feynman diagram which includes only quark lines) known in QCD [33]. Resembling standard Feynman diagrams in quantum field theories, an antivortex is represented by a line with an arrow opposite to the time evolution. Thus, we find a four meson vertex as an elemental interaction among mesons.

The second process, corresponding to Fig. 14(b) is essentially the same as in Fig. 14(a). So the scattering in Fig. 14(b) is also described by the same four-meson vertex in Fig. 15.

Next, let us make a diagram for the third process, shown in Fig. 14(c). This scattering is more complicated. Indeed, the corresponding reaction formula given in Eq. (21) consists of three proceeding steps. The Feynman diagram for this scattering is given in Fig. 16 including a loop and three different 3-vertices. The leftmost vertex of Fig. 16 is a meson-meson-meson where all mesons are of the u type, as shown as Fig. 17(a). The middle and rightmost vertices are meson-baryon-baryon vertices, summarized as Figs. 17(b) and 17(c).

Once we get these elementary vertices, it is straightforward for us to expect what kind of scattering events are possible without performing numerical simulations. Therefore, our next task is to track down all possible vertices. To this end, symmetry is helpful. Our system has the symmetry $F : \Psi_1 \leftrightarrow \Psi_2$ due to the special choice of the parameters given in Eq. (2). This ensures the "flavor" symmetry among the vortices as $F : (X_u(t), Y_u(t)) \leftrightarrow (X_d(t), Y_d(t))$, where $(X_{u,d}(t), Y_{u,d}(t))$ denotes the position of a u- or d-vortex at time $t$. Furthermore, the GP equations are invariant under the time-reversal symmetry $T : \Psi_i(x_1, x_2, t) \leftrightarrow \Psi_i^*(x_1, x_2, -t)$, and the parity transformation $P : \Psi_i(x_1, x_2, t) \leftrightarrow \Psi_i(x_1, -x_2, t)$. Note that the parity transformation in even spatial dimensions is identical to a reflection symmetry on an axis. With respect to the vortices, the former transforms a u-vortex to a $\bar{u}$-vortex as $T : (X_u(t), Y_u(t)) \leftrightarrow (X_{\bar{u}}(-t), Y_{\bar{u}}(-t))$. The same holds for d- and $\bar{d}$-vortices. Similarly, the latter also transforms

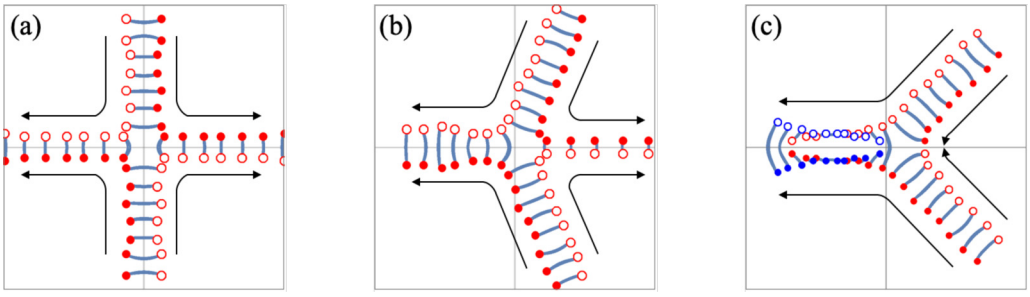


FIG. 14. Summary of u meson and u meson collider experiments: (a) corresponds to Fig. 6, (b) to Fig. 10, and (c) to Fig. 12. The plot region is $\tilde{x}_1 \in [-40, 40]$ (horizontal) and $\tilde{x}_2 \in [-40, 40]$ (vertical).

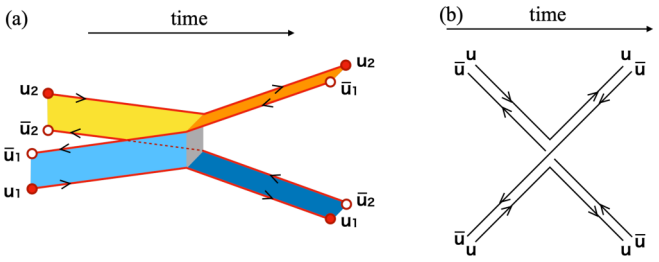


FIG. 15. Meson-meson-meson-meson vertex: The left panel is a 3D diagram that describes (a) in Fig. 14. The right panel is a Feynman diagram, which is a simplified 2D expression of the left one.

a u-vortex to ū since it exchanges $\theta = \arg(x_1 + ix_2) \leftrightarrow -\theta = \arg(x_1 - ix_2)$. Hence, the parity transformation is $P$ : $(X_u(t), Y_u(t)) \leftrightarrow (X_{\bar{u}}(t), -Y_{\bar{u}}(t))$ and similar for d- and d̄-vortices. By using the $F$, $T$, and $P$ transformations, we can exhaust all possible diagrams as summarized in Fig. 18. For example, the diagrams labeled by (mmmm1) and (mmmm2) are exchanged by the $F$ transformation, while those labeled by (mmm1) and (mmm3) are related by the $T$ transformation. All the diagrams in Fig. 18 are invariant under the $P$ transformation.

### E. ūu-ūu collisions with impact parameters

The final process for the ūu-ūu collisions are scatterings with impact parameters. The initial mesons are placed at $(\tilde{x}_1, \tilde{x}_2) = (\pm\tilde{b}, 50)$. First, we horizontally shift the initial mesons of Fig. 6 by $\tilde{b} = 2.5$ as shown in Fig. 19. The scattering follows similarly to the head-on collision shown in Fig. 6 except for a scattering angle. As can be seen in the panel for $\tilde{t} = 100$ in Fig. 19, the new mesons created after the recombination are not vertical but diagonal.

As is naturally expected, the scattering angle gets smaller as the impact parameter becomes larger. Figure 20 shows a scattering with impact parameter $\tilde{b} = 5$. Namely, the two mesons are not initially overlapped horizontally. Nevertheless, the recombination occurs during the collision, and the mesons collide with a negative scattering angle.

If we initially place the mesons instead with a larger impact parameter, then they pass through each other almost without interactions. Figure 21 shows the scattering with the impact parameter $\tilde{b} = 7.5$. The mesons go almost straight with a negative but small scattering angle. This suggests that the asymptotic meson-meson interaction is attractive. We summarize the scatterings with impact parameters $\tilde{b} = 0$, 2.5, 5, and 7.5 in Fig. 22.

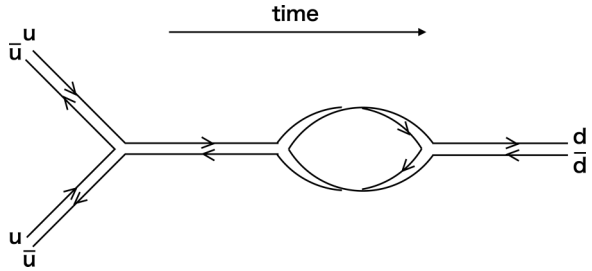


FIG. 16. The one-loop diagram for ūu + ūu → d̄d corresponding to Fig. 14(c).

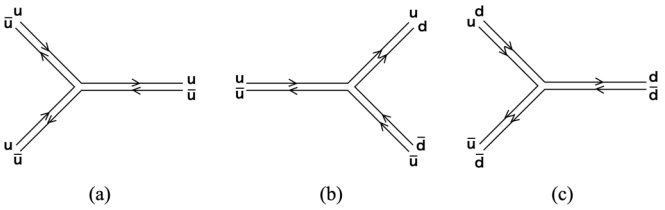


FIG. 17. The three 3-vertices included in the one-loop diagram in Fig. 16. The time direction is from left to right.

## IV. MESON-MESON SCATTERING: THE CASE OF ūu-d̄d

### A. ūu-d̄d head-on collision at zero angle

Let us next study the scatterings of a u meson and a d meson. We first collide the two mesons head on. The initial configuration is prepared by superposing a u meson at $(\tilde{x}_1, \tilde{x}_2) = (0, 50)$ and the d meson at $(\tilde{x}_1, \tilde{x}_2) = (0, -50)$ [precisely speaking, we put a u-vortex at $(\tilde{x}_1, \tilde{x}_2) = (5, 50)$ and a ū-vortex at $(\tilde{x}_1, \tilde{x}_2) = (-5, 50)$, and a d-vortex at $(\tilde{x}_1, \tilde{x}_2) = (-5, -50)$ and a d̄-vortex at $(\tilde{x}_1, \tilde{x}_2) = (5, -50)$]. The result of this scattering event is shown in Fig. 23, which one might think is not so interesting compared to the ūu-ūu head-on collision given in Fig. 5. Indeed, the two mesons seem to pass through without an interaction, see Figs. 23 and 24. This observation is true if we look at only the vortices. However, it is not true for the SG solitons. As can be seen from Fig. 23, this scattering can be understood as a collision of one SG soliton (belonging to the u meson) and the other SG soliton (belonging to the d meson). This can be seen by noting that the color orders along the $\tilde{x}_2$ axis are the same for the u and d mesons. This situation is in contract to the meson-meson

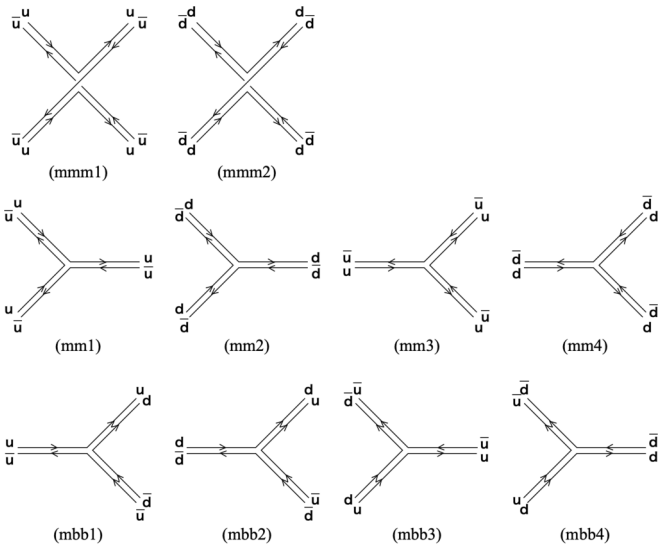


FIG. 18. Feynman diagrams found in two u (d) meson scattering experiments. The first row shows the meson-meson-meson-meson vertices. The second row shows the meson-meson-meson vertices, and the third row shows the meson-baryon-baryon vertices.

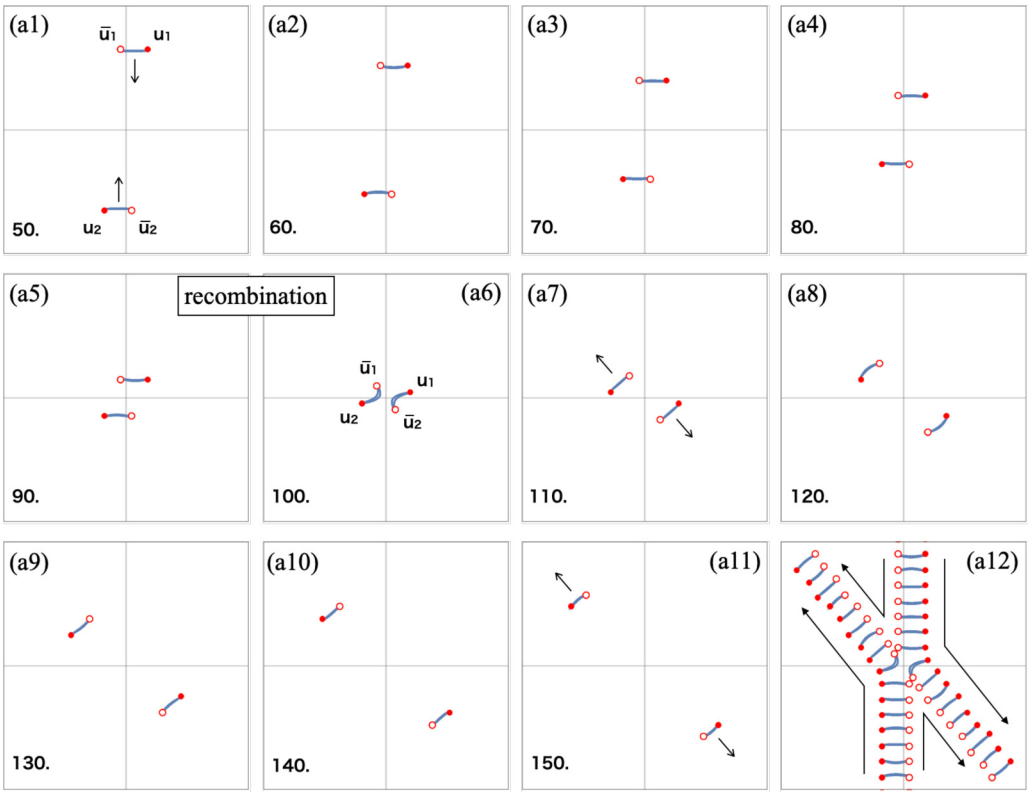


FIG. 19. Meson-meson scattering (ūu-ūu) with an impact parameter. Initially, the two mesons are placed at $(\tilde{x}_1, \tilde{x}_2) = (\tilde{b}, 50)$ and $(-\tilde{b}, 50)$ with the impact parameter $\tilde{b} = 2.5$. We show the snap shots with $\tilde{t} = 50 \sim 150$ with interval $\delta\tilde{t} = 10$. The panel at the bottom right corner is a sequence of meson trajectories from the incoming and out-going collision. The plot region is $\tilde{x}_1 \in [-40, 40]$ (horizontal) and $\tilde{x}_2 \in [-40, 40]$ (vertical).

scattering in Fig. 5 in which the SG and anti-SG solitons approach each other.

To see a nontrivial phenomenon in this scattering, let us carefully observe the period of passing. Figure 25 shows zoomed snapshots at $\tilde{t} = 97.5, 100, 102.5, 105$. While the u- and $\bar{\text{d}}$- (d- and ū-)-vortices pass through each other, the SG solitons largely bend toward the opposite direction compared to Fig. 7 due to repulsive interaction between the SG solitons. Thus, the distance between two SG solitons at the center of mesons never vanishes, and the SG solitons backscatter. Figure 26 shows the relative phase $\arg(\Psi_1) - \arg(\Psi_2)$ on the $\tilde{x}_2$ axis. Throughout the scattering, there always exist two SG solitons (corresponding to phase jumps from $-\pi \to \pi$). Since they are topologically protected, they cannot be annihilated. This is why their distance does not vanish and they backscatter.

Thus, we found that the SG solitons backscatter, whereas the vortices at the ends of mesons pass through each other. Along with this observation, we conclude that the mesons interchange the SG solitons before and after the head-on collision.

### B. ūu-$\bar{\text{d}}$d scattering at $\pi/8$ angle

The collision of the u and d mesons studied in the previous section is not so interesting in the sense that it does not include recombination phenomena which commonly occurs for the u and u meson scatterings. To see whether the recombination is specific to the u and u meson scattering only, or if it is a general effect for most scattering events, let us investigate the collision of the u and d mesons at finite angles here and in the next subsection.

Figure 27 shows the outlook of the head-on collision of the u and d mesons with angle $\pi/8$. Compared to Fig. 9, the lower ūu meson is replaced by $\bar{\text{d}}$d. At a first glance, the mesons seem to just pass through each other, just as the previous scattering in Fig. 23. However, it is actually not so trivial. Since the mesons are tilted, there is a certain period during which the u-vortex at the lower edge of the u meson and the $\bar{\text{d}}$-vortex at the upper edge of the d meson exchange their positions, while the remaining constituent vortices are left unchanged, see the snapshot at $\tilde{t} = 100$ of Fig. 28. Soon after, the second passing of the remaining ū- and d-vortices follows; see the snapshot at $\tilde{t} = 110$ of Fig. 28. The interchange of constituent vortices is accompanied by the recombination of the SG solitons. During the period between the first and the second recombinations, the molecules are not u and d mesons but the baryon ud and antibaryon ū$\bar{\text{d}}$. Indeed, the SG solitons bridge the u- and d-vortices (ū- and $\bar{\text{d}}$-vortices) in the snapshot at $\tilde{t} = 100$ in Fig. 28.

Thus, the simulation here implies that the recombination can happen universally not only for the mesons of the same species but also for the different species. We have not observed the recombination presented in Fig. 23, because the two mesons are placed to be exactly parallel during collision dynamics.

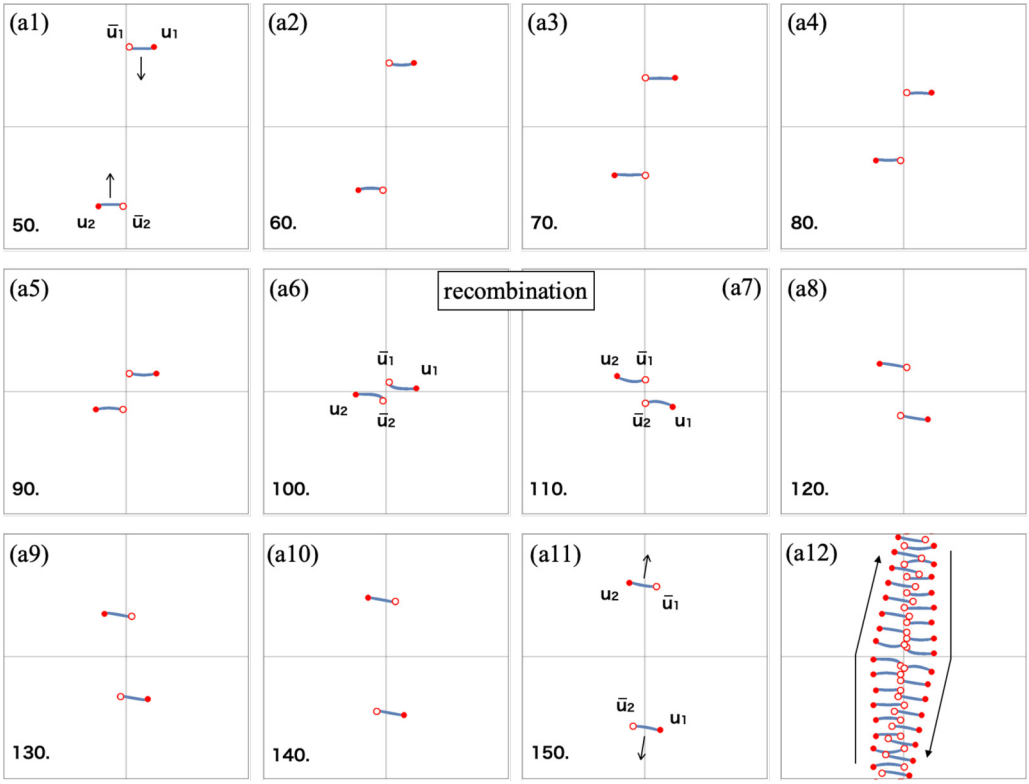


FIG. 20. Meson-meson scattering (ūu-ūu) with an impact parameter. Initially, the two mesons are placed at $(\tilde{x}_1, \tilde{x}_2) = (\pm\tilde{b}, 50)$ with the impact parameter $\tilde{b} = 5$. We show the snapshots with $\tilde{t} = 50$-$150$ with interval $\delta\tilde{t} = 10$. The panel at the bottom right corner is a sequence of meson trajectories from the incoming and out-going collision. The plot region is $\tilde{x}_1 \in [-40, 40]$ (horizontal) and $\tilde{x}_2 \in [-40, 40]$ (vertical).

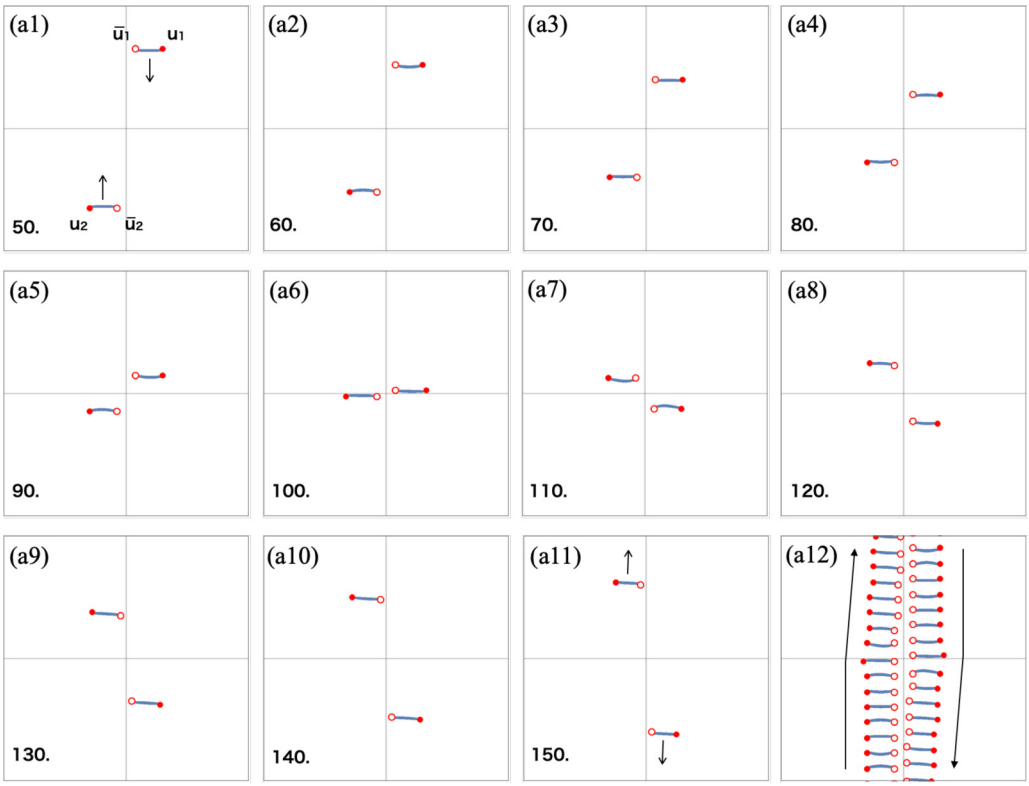


FIG. 21. Meson-meson scattering (ūu-ūu) with an impact parameter. Initially, the two mesons are placed at $(\tilde{x}_1, \tilde{x}_2) = (\pm\tilde{b}, 50)$ with the impact parameter $\tilde{b} = 7.5$. We show the snapshots with $\tilde{t} = 50 \sim 150$ with interval $\delta\tilde{t} = 10$. The panel at the bottom right corner is a sequence of meson trajectories from the incoming and out-going collision. The plot region is $\tilde{x}_1 \in [-40, 40]$ (horizontal) and $\tilde{x}_2 \in [-40, 40]$ (vertical).

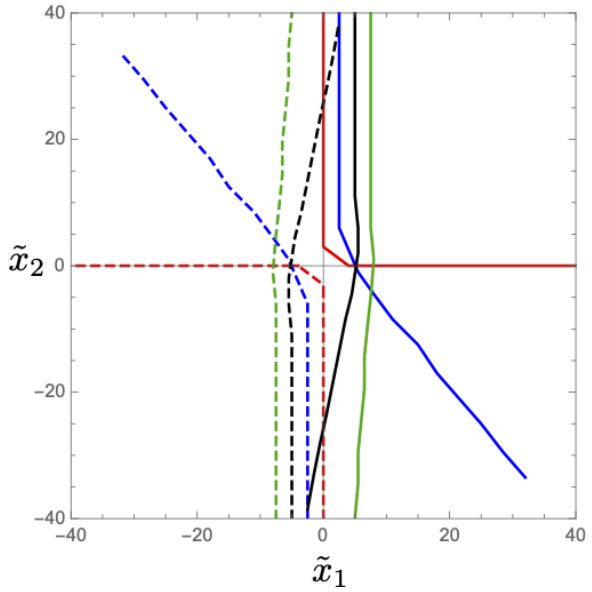


FIG. 22. The orbits (red, blue, black, and green) of centers of the mesons during the meson-meson scatterings with the impact parameters $\tilde{b} = 0, 2.5, 5$, and 7.5 corresponding to Figs. 6, 19, 20, and 21, respectively.

Let us cut out the period with created baryons and see their motion in more detail. Figure 29 shows zoomed snapshots for $\tilde{x}_i \in [-15, 15]$ at $\tilde{t} = 97.5, 100, 102.5, 105$, and 107.5. The baryon (antibaryon) formed after the first recombination rotates counterclockwise (clockwise) until they are reformulated back into the mesons. During the period with baryons, they almost do not propagate. As a consequence, the meson orbits before and after the collision slightly shift due to delay of forming baryons.

### C. ūu-d̄d scattering at $\pi/4$ angle

The observations in the previous subsection can be more sharply seen in the scattering of the u and d mesons with larger angle; we take $\pi/4$ here as an example. Figure 30 shows an outlook of the scattering process. Qualitatively, it goes very similarly to that with the angle $\pi/8$ given in Fig. 28. Namely, the incoming u and d mesons are converted to the intermediate baryon and antibaryon pair at the first recombination. The baryons rotate at their position without propagating for a while. Then they are reformed back into the mesons at the second recombination and propagate linearly toward the boundary. However, the baryonic period in this scattering is longer than the previous one because of the steeper angle of the incoming mesons. Comparing Figs. 29 and 31, the baryonic period is $\tilde{t} \simeq 97.5$–$105$ for the former while $\tilde{t} \simeq 95$–$107.5$ for the latter. A longer lifetime of the baryonic period makes the rotation of the baryons easier to discern.

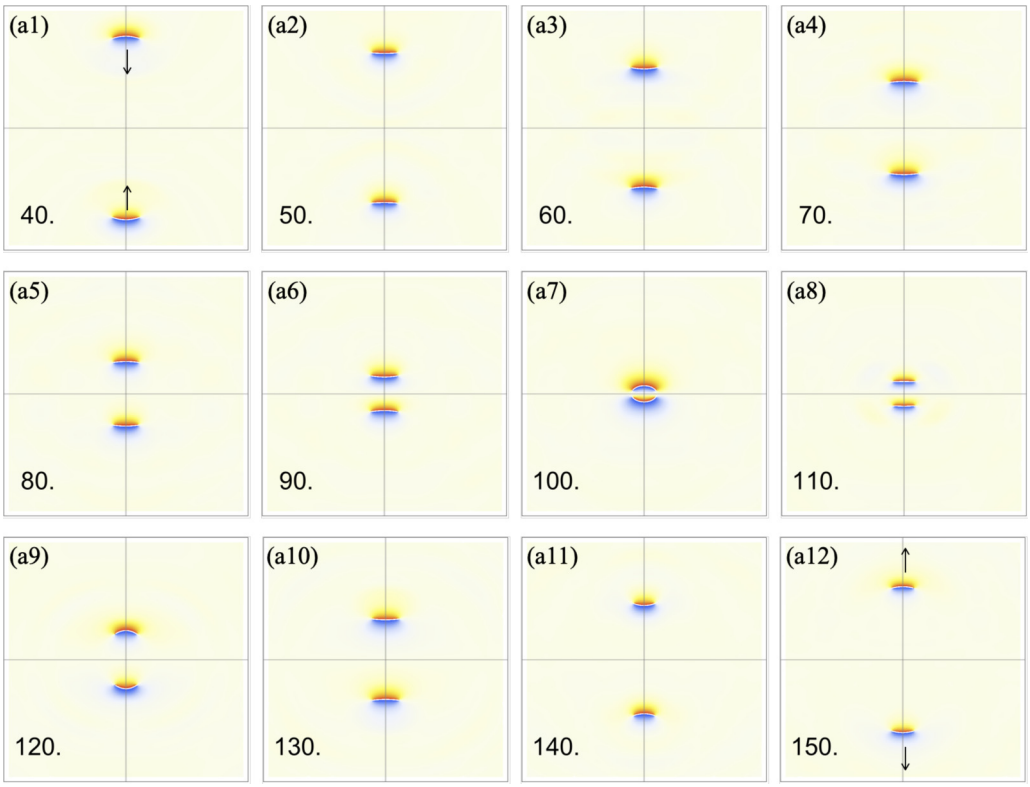


FIG. 23. The u and d meson scattering: Color density plots of the relative phase $\arg(\Psi_1) - \arg(\Psi_2)$. We initially ($\tilde{t} = 0$) set the u meson at $(\tilde{x}_1, \tilde{x}_2) = (0, 50)$ and the d meson at $(\tilde{x}_1, \tilde{x}_2) = (0, -50)$. They linearly propagate with almost constant speeds and pass through each other without an interaction. We show the snapshots from $\tilde{t} = 40$ to 150 with interval $\delta\tilde{t} = 10$ and the plot region is $\tilde{x}_1 \in [-40, 40]$ (horizontal) and $\tilde{x}_2 \in [-40, 40]$ (vertical).

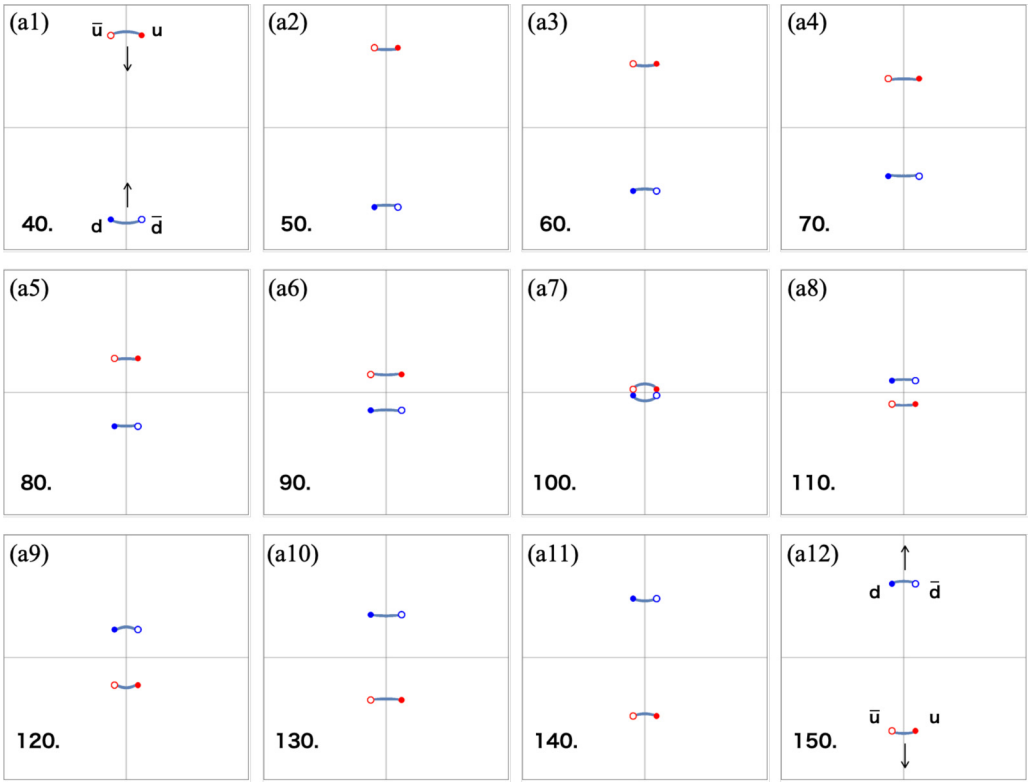


FIG. 24. A simplified plot of the u meson and d meson scattering shown in Fig. 23. We put filled red circles (open red circles) at the points corresponding to the u- (ū-)-vortex centers. Similarly, we put filled blue circles (open blue circles) at the points corresponding to the d- ($\bar{\text{d}}$-)-vortex centers. Gray regions bridging the u- and ū-vortices (d and $\bar{\text{d}}$) show the SG solitons. The gray regions are those where the relative phases take the values within $3 \leqslant |\arg(\Psi_1) - \arg(\Psi_2)| \leqslant \pi$.

As mentioned, the conversion of mesons to baryon and antibaryon results in a delay of the orbits of the incoming and outgoing mesons. In order to see the delay clearly, we show a sequence of trajectories for the u and d meson scatterings with $\pi/8$ and $\pi/4$ angles in Fig. 32. One can see the orbits of the constituent vortices steeply bend at the timing of recombinations. Since vertical motions of the vortices in Fig. 32 are simple shifts with almost constant speed, we can approximately

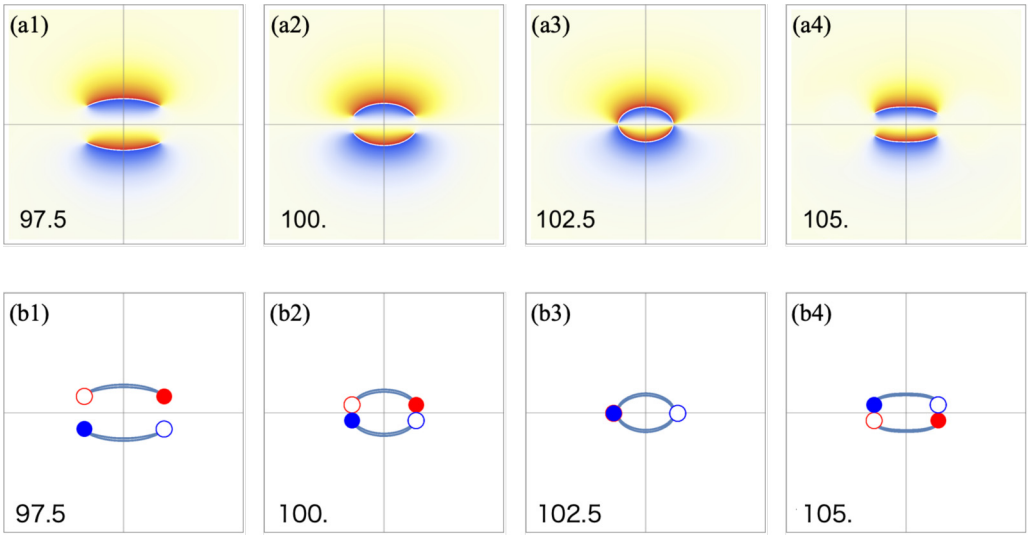


FIG. 25. Zoomed snapshots for the horizontal region $\tilde{x}_1 \in [-15, 15]$ and the vertical region $\tilde{x}_2 \in [-15, 15]$ at $\tilde{t} = 97.5, 100, 102.5, 105$ for the u meson and d meson scattering given in Figs. 23 and 24. The SG solitons from the top and bottom gradually bend as they approach each other by and backscatter, whereas the vortices at the ends of the mesons pass through each other. As such, the mesons interchange the SG solitons during the collision.

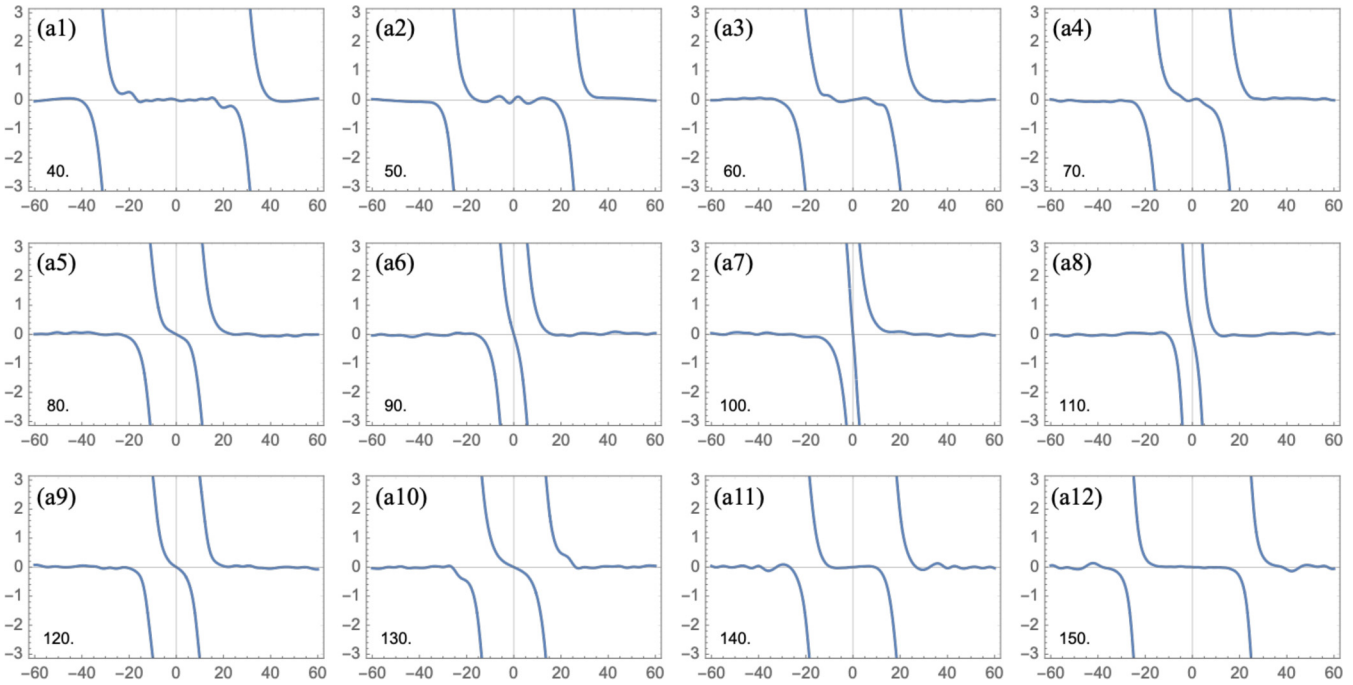


FIG. 26. The solid blue curve shows the relative phase $\arg(\Psi_1) - \arg(\Psi_2)$ along the $\tilde{x}_2$ axis of Fig. 23. The SG solitons coming from the right- and left-hand sides collide and scatter backward. Throughout the scattering, the SG winding number ($n_S = 2$) is preserved.

regard the vertical axis as time. Then the horizontal motions would be interpreted as a phase shift which commonly appears in soliton scatterings or particle scattering. The phase shift in our system is due to the formation of unstable intermediate baryonic states with finite lifetime. It is interesting that a phase shift common for scattering is observed here, although the

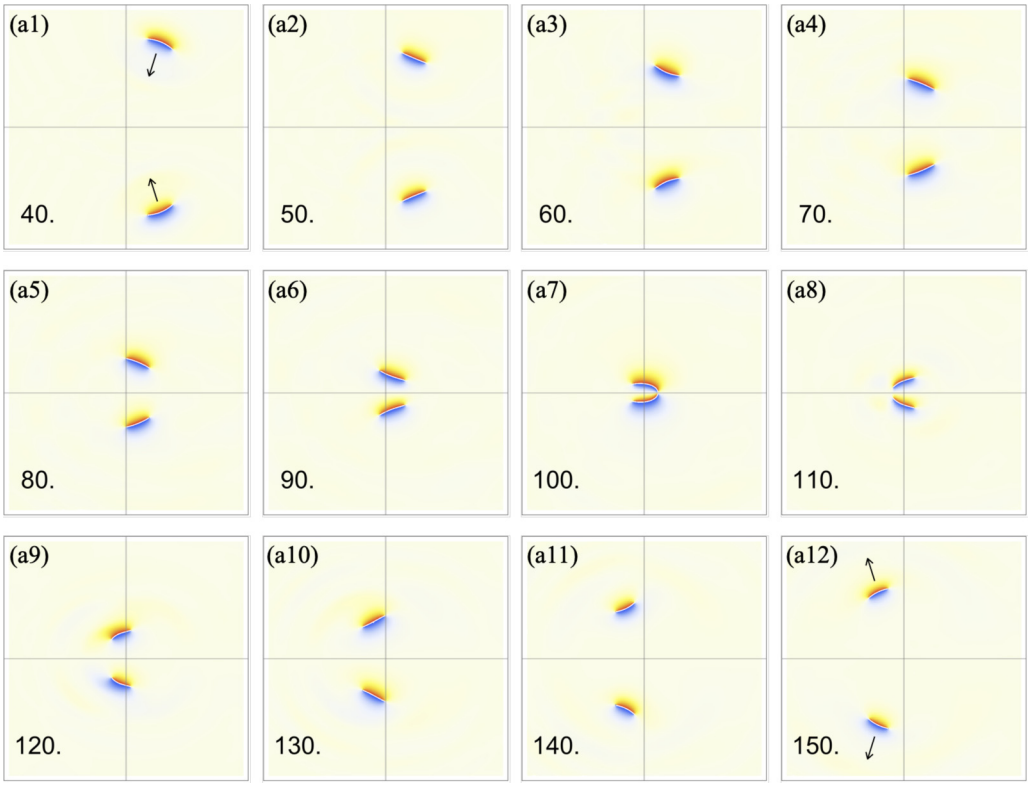


FIG. 27. Scattering of the slightly tilted u and d mesons with angle $\pi/8$. We initially ($\tilde{t} = 0$) set the u meson at $(\tilde{x}_1, \tilde{x}_2) = (50\sin\pi/8, 50\cos\pi/8)$ and the d meson at $(\tilde{x}_1, \tilde{x}_2) = (50\sin\pi/8, -50\cos\pi/8)$. We only show the snapshots from $\tilde{t} = 40$ to 150 with interval $\delta\tilde{t} = 10$, and the plot region is $\tilde{x}_1 \in [-40, 40]$ (horizontal) and $\tilde{x}_2 \in [-40, 40]$ (vertical).

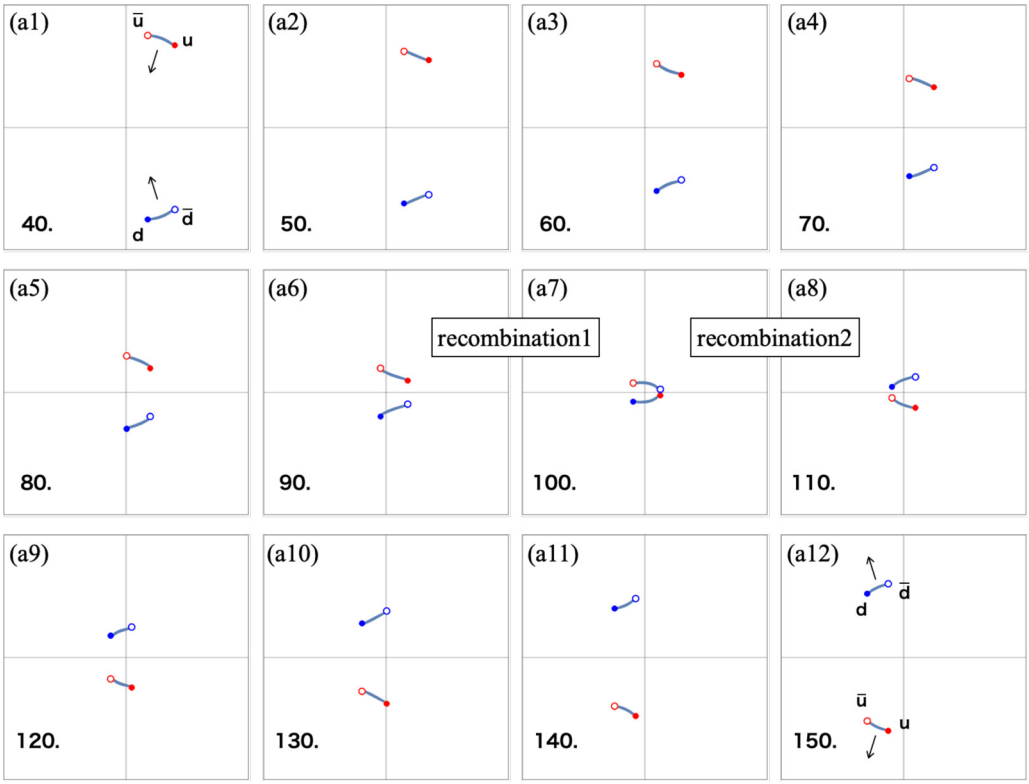


FIG. 28. A simplified plot of the u mesons scattering shown in Fig. 27.

mechanism is specific to our system and has not been reported elsewhere.

### D. Interaction vertices and Feynman diagrams

As in the u and u mesons scattering, we can interpret u and d mesons scattering with Feynman diagram. The diagram for Fig. 32 is a one-loop diagram given in Fig. 33(a). It includes meson-meson-baryon-baryon vertices which are shown in Figs. 33(b) and 33(c). They are invariant under the $F$ and $P$ transformations while they are exchanged by the $T$ transformation. Hence, no more diagrams are generated by the symmetries.

Related to these meson-meson-baryon-baryon vertices, we observed in our previous work Ref. [16] that a long meson disintegrates into three short molecules as

$$\bar{u}u \to ud + \bar{d}d + \bar{d}\bar{u}. \tag{22}$$

The Feynman diagrams corresponding to this and other related diagrams via the $F$, $T$, and $P$ symmetries are presented

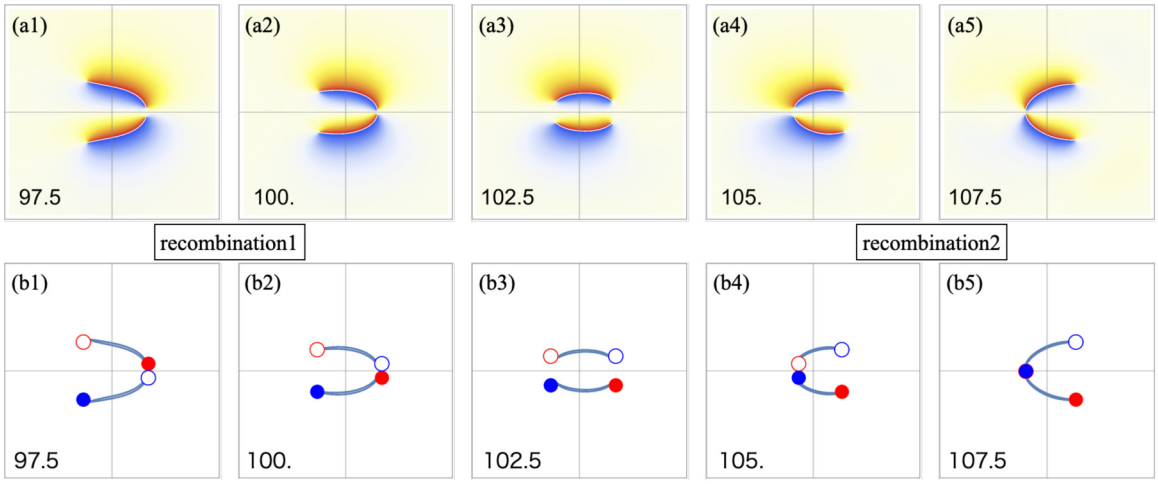


FIG. 29. Zoomed snapshots for the horizontal region $\tilde{x}_1 \in [-15, 15]$ and the vertical region $\tilde{x}_2 \in [-15, 15]$ at $\tilde{t} =$ 97.5, 100, 102.5, 105, 107.5 for the u meson and d meson for scattering events presented in Figs. 27 and 28. The mesons are converted into a baryon and antibaryon pair for a short period.

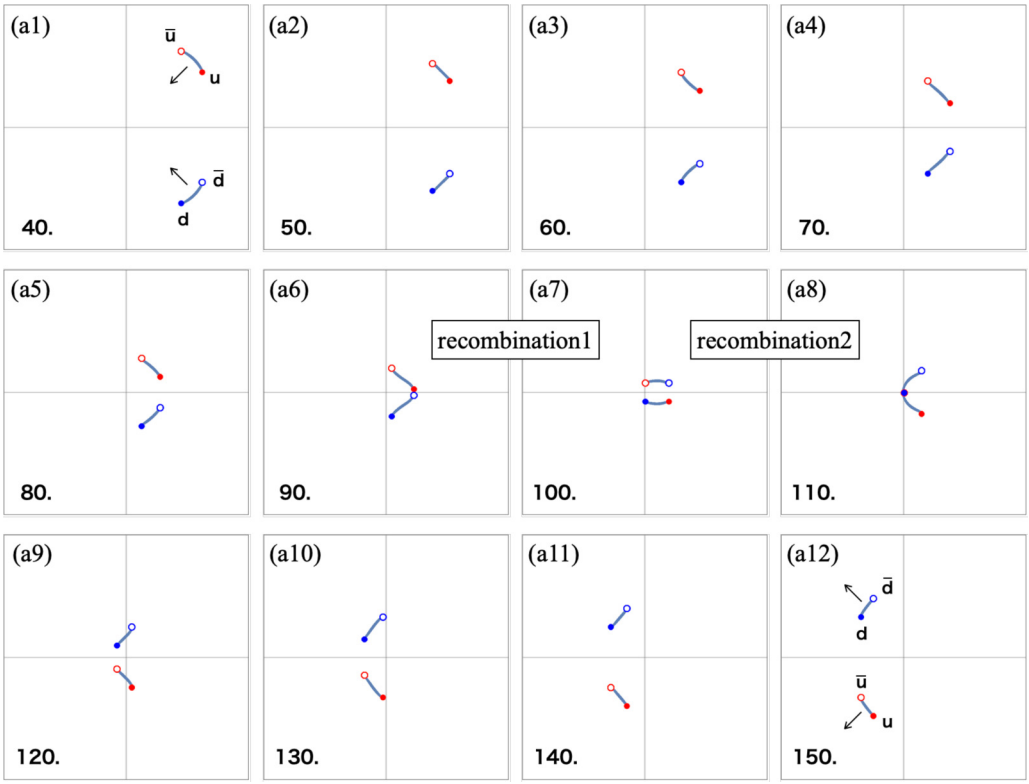


FIG. 30. Scattering of the tilted u and d mesons with angle $\pi/4$. We initially ($\tilde{t} = 0$) set the u meson at $(\tilde{x}_1, \tilde{x}_2) = (50 \sin \pi/4, 50 \cos \pi/4)$ and the d meson at $(\tilde{x}_1, \tilde{x}_2) = (50 \sin \pi/4, -50 \cos \pi/4)$. We only show the snapshots from $\tilde{t} = 40$ to 150 with interval $\delta\tilde{t} = 10$, and the plot region is $\tilde{x}_1 \in [-40, 40]$ (horizontal) and $\tilde{x}_2 \in [-40, 40]$ (vertical).

in Fig. 34. Interestingly, these diagrams can be generated by horizontally flipping an external leg of Figs. 33(b) and 33(c). In a usual relativistic quantum field theory, the presence of the vertex in Fig. 33(b) immediately means that the vertex of the leftmost panel of Fig. 34 also exists as either a real or virtual process. However, our theory here is not relativistic, and, moreover, we are dealing with only real processes which are solution of the GP equations. Therefore, for our system, the vertex in Fig. 33(b) does not automatically ensure the vertex of the leftmost panel of Fig. 34. We should emphasize that we put the four diagrams of Fig. 34 in our list of the real processes because we found them in real dynamics. To make

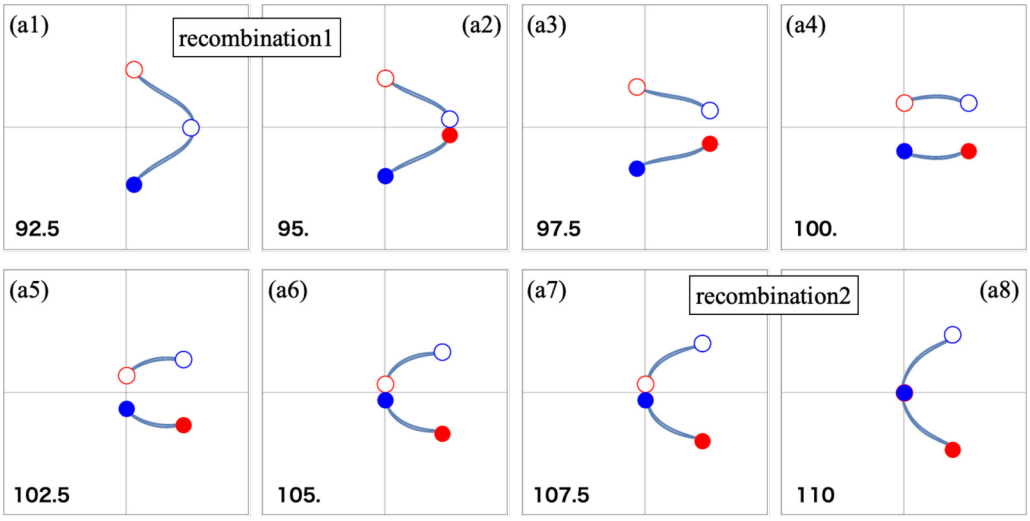


FIG. 31. Zoomed snapshots for the horizontal region $\tilde{x}_1 \in [-15, 15]$ and the vertical region $\tilde{x}_2 \in [-15, 15]$ at $\tilde{t} = 92.5, 95, 97.5, 100, 102.5, 105, 107.5, 110$ for the u meson and d meson scattering given in Fig. 30.

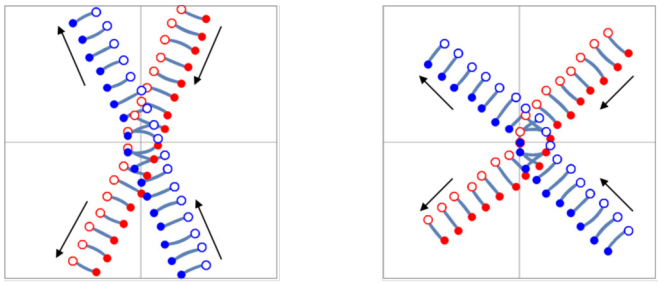


FIG. 32. Meson scattering trajectories for the u and d meson scatterings with $\pi/8$ and $\pi/4$ angles given in Figs. 28 and 30. The plot region is $\tilde{x}_1 \in [-40, 40]$ (horizontal) and $\tilde{x}_2 \in [-40, 40]$ (vertical).

this contrast clearer, let us mention another process which we previously encountered in Refs. [14,16]:

$$\mathrm{ud} \to \mathrm{ud} + \bar{\mathrm{d}}\bar{\mathrm{u}} + \mathrm{ud}. \tag{23}$$

The corresponding Feynman diagram and the other diagrams obtained via the $F$, $T$, and $P$ transformations are given in Fig. 35. By flipping the out-going external ud leg of the leftmost diagram in Fig. 35, we can generate the diagram shown in the left panel of Fig. 36. However, a real process corresponding to this diagram does not seem to happen. This is because a baryon ud and an antibaryon $\bar{\mathrm{u}}\bar{\mathrm{d}}$ are a pair formed from an integer vortex and an antivortex, so that they move parallel with their distance kept constant, as can be seen in the right panel of Fig. 36. Hence, we have learned that we cannot freely flip any external legs of a vertex from left (right) to right (left).

### E. ūu-d̄d collisions with impact parameters

To make our study self-contained, let us repeat the same simulations for $\bar{\mathrm{u}}\mathrm{u}$ and $\bar{\mathrm{d}}\mathrm{d}$, as those for $\bar{\mathrm{u}}\mathrm{u}$ and $\bar{\mathrm{u}}\mathrm{u}$ in Sec. III E. Namely, we study the u and d mesons collisions with the impact parameter $\tilde{b}$. As counterparts of Figs. 19, 20, and 21, we do the same simulations by replacing the lower $\bar{\mathrm{u}}\mathrm{u}$ meson with the $\bar{\mathrm{d}}\mathrm{d}$. The results are shown in Figs. 37, 38, and 39. Comparing Figs. 21 and 39, it turns out that the asymptotic interaction between the u and d mesons are much smaller than the one between the u and u mesons. Therefore, we see that the contact interaction dominates for the former.

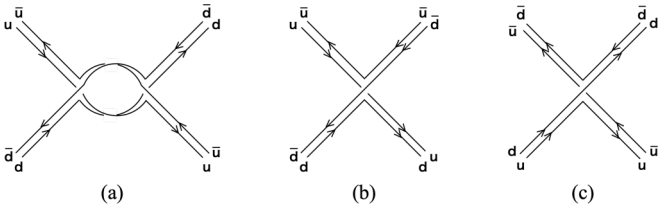


FIG. 33. (a) The Feynman diagram corresponding to the real processes in Fig. 30. [(b) and (c)] The meson-meson-baryon-baryon vertices which are building blocks of the twig diagram (a).

## V. BARYON-MESON SCATTERING

Our final vortical collider simulations are simulations of scattering between a meson and a baryon. Since baryons do not propagate linearly but instead rotate, we put a baryon at the origin as a target. Then we put an incoming meson sufficiently far from the target baryon, and they collide in a similar manner to our other collider experiments. As expected, details of the scatterings sensitively depend on the timings of collision, namely geometric information such as relative positions and angles of the baryon and meson. It is impossible to simulate all cases, and so we introduce two typical collision simulations which illustrate general features. In addition, we exhibit one more example which has a special phenomenon, a jet, which is reminiscent of hadron collider experiments.

### A. Typical collisions

In this subsection, we exhibit two scattering simulations whose initial configurations are given in Figs. 40(a) and 40(b). For both instances, we put the same meson as the one given in Fig. 4 at $(\tilde{x}_1, \tilde{x}_2) = (50, 0)$. Similarly, the same baryon as the one given in Fig. 4 is located at the origin. The meson propagates toward the target baryon rotating at the origin. The difference between Figs. 40(a) and 40(b) is that the initial angles of the target baryon are different by 180°, so that the relative positions of the meson and baryon at the moment of collision are different.

In Fig. 41, the scattering from the initial configuration in Fig. 40(a) is shown. The u meson approaches the rotating target baryon and they collide. After the collision, a u meson propagates with a scattering angle of about 45° while the baryon is left near the origin. This corresponds to the scattering event $\bar{\mathrm{u}}\mathrm{u} + \mathrm{ud} \to \bar{\mathrm{u}}\mathrm{u} + \mathrm{ud}$ which one might find nothing interesting. However, as for the case of the meson-meson scatterings, it is not so simple. One nontrivial phenomena that occurs here is the recombination before and after the collision. As can be seen in the panels with the time stamps $\tilde{t} = 90$ and 100, the meson and baryon exchange the u constituent vortices. Therefore, both the meson and baryon after the collision are different from those before the collision. If we express the initial meson as $\bar{\mathrm{u}}_1\mathrm{u}_1$ and the initial baryon as $\mathrm{u}_2\mathrm{d}$, then the process can be summarized as the following vortical reaction:

$$\bar{\mathrm{u}}_1\mathrm{u}_1 + \mathrm{u}_2\mathrm{d} \to \bar{\mathrm{u}}_2\mathrm{u}_1 + \mathrm{u}_1\mathrm{d}. \tag{24}$$

To understand this better, let us carefully look at the collision period. Figure 42 shows zoomed snapshots for $\tilde{x}_i \in [-15, 15]$ around the collision. We find that the snapshots are qualitatively the same as those given in Fig. 7 for the ūu-ūu scattering. As before, the recombination takes place together with partial annihilation of the SG and anti-SG solitons.

The other scattering from the initial configuration Fig. 40(b) is also shown in Fig. 43. The scattering goes almost the same as the previous one. The u meson collides with the target baryon, and a u meson is scattered while a baryon is left near the origin. The scattering angle is now about −45°. The difference of the scattering angles is just due to the relative position and angle of the meson and baryon at the moment of the collision. Similarly to the first simulation,

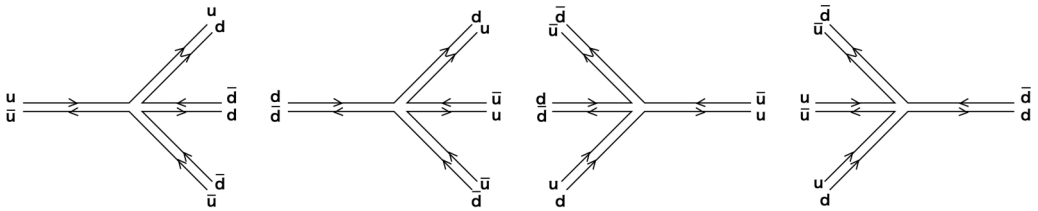


FIG. 34. The meson-meson-baryon-baryon vertices correspond to and relate to a long meson disintegration into a baryon, an antibaryon, and a meson.

the meson and baryon experience the recombination once during the collision. Therefore, the vortical reaction is the same as Eq. (24). Nevertheless, detailed dynamical processes of the recombination are not the same. To see the difference clearer, let us zoom in on the collision moment shown in Fig. 44. Unlike the previous case, the collision is accompanied not by the SG and anti-SG solitons but the SG and SG solitons. Hence, the recombination here is very similar to what we saw in Fig. 25 for the $\bar{u}u$ and $\bar{d}d$ meson scattering. Since the two SG solitons repel each other, they cannot be close. Only one set of the edges of the meson and baryon come across to exchange $\bar{u}_1$ of $\bar{u}_1 u_1$ and d of $u_2 d$. Then a new meson $\bar{u}_1 u_2$ goes away and a new baryon $u_1 d$ remains near the origin and keeps rotating. We have examined lots of collisions with various initial configuration and have found that all of them are qualitatively the same.

### B. A vortical hadron jet

In high-energy physics, when hadrons collide with sufficiently high energy, they fragment into quarks or gluons. However, obeying the color confinement in QCD, no color charged objects can exist alone. Therefore, these fragments create new colored particles around them to form color neutral objects, namely hadrons. A bunch of the hadrons forming a narrow beam is called a hadron jet. Since our vortices also obey the $U(1)_R$ confinement in BECs, which as we have seen is quite similar to QCD, we expect that a hadron jet could be observed also in BECs.

The propagation speed of a vortical meson is determined by the length of the meson. Namely, we cannot freely change the propagation speed of the mesons unlike relativistic particles in reality. The shorter the meson is, the faster it propagates. However, there is a threshold of the minimum length of the meson over which mesons are unstable to annihilate. Therefore, we cannot give a large initial kinetic energy to individual mesons. Hence, it is not easy to set up a simulation with arbitrary high colliding energies in BECs. Indeed, as we have seen in the previous subsections so far, the typical scatterings do not yield any additional new hadrons. Consequently, we change our strategy: Instead of using shorter mesons, we take longer mesons. Thus, we prepare the third initial configuration given in Fig. 40(c) in which the baryon is the same as Fig. 40(a) but the meson is longer. It is shown in Fig. 45 how the collision of a longer meson and normal baryon occurs. Since the longer meson propagate at a slower rate, it takes more time to reach the target baryon at the origin. Thus, compared with Fig. 41, the baryon rotates slightly more so that the relative angle between the meson and baryon is also slightly different. However, the first reaction is not affected by such a small difference. Namely, the meson and baryon again experience the recombination accompanied by a partial annihilation of the SG and anti-SG solitons. While the corresponding vortical reaction process is the same as Eq. (24), the details of the collision are shown in Fig. 46. As before, a relatively short meson $\bar{u}_1 u_2$ and a relatively long baryon $u_1 d_1$ form during the collision. The former flies away with a smaller scattering angle. The latter baryon is very long and bent. Then it soon disintegrates into smaller hadrons. Indeed, it fragments by creating a $d_2$ and $\bar{d}_2$ at a certain point at the middle of the longer baryon. As a consequence, the third hadron, $\bar{d}_1 d_2$ is emitted toward a similar direction of the first meson $\bar{u}_1 u_2$. We interpret the new hadron which appears as a result of fragmentation of the confining SG soliton a vortical hadron jet, though the jet consists of only two mesons $\bar{u}_1 u_2$ and $\bar{d}_2 d_1$. The vortical reaction for it is

$$d_1 u_1 \to \bar{d}_2 d_1 + u_1 d_2. \tag{25}$$

The third meson $\bar{d}_2 d_1$ is very short. So it crawls under waves of $\Psi_i$ for a while and soon emerges again, see the panels with $\tilde{t} = 130$ and 140 in Fig. 45.

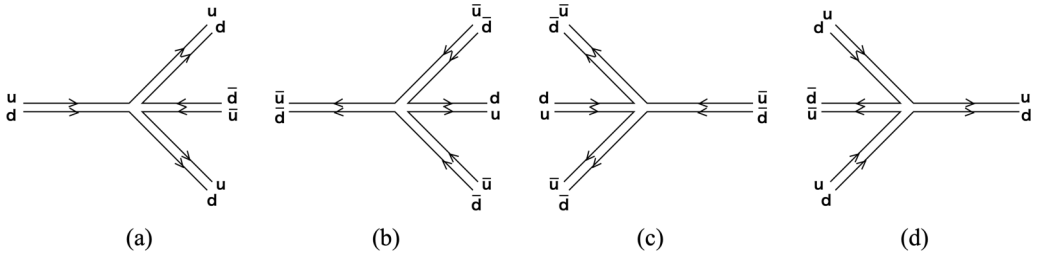


FIG. 35. The baryon-baryon-baryon-baryon vertices correspond to and relate to a long baryon disintegration into two baryons and one antibaryon.

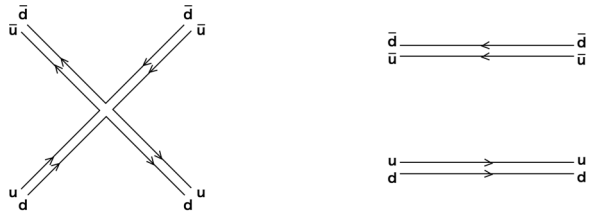


FIG. 36. The baryon-baryon-baryon-baryon vertices correspond to and relate to a long baryon disintegration into two baryons and an antibaryon.

### C. Feynman diagrams

We have found the two new vortical reactions summarized in Eqs. (24) and (25) through meson-baryon scattering. They can also be described by Feynman diagrams as before. The corresponding diagrams are a meson-meson-baryon-baryon vertex and a meson-meson-baryon vertex as shown in Fig. 47. The former vertex is new in a sense that any of the discrete symmetries $F$, $T$, and $P$ cannot relate it to any of the previous diagrams shown so far. Although the latter vertex has not also been encountered before, it can be obtained by flipping an external leg of the vertex (mbb4) of Fig. 18. However, as mentioned, the presence (mbb4) of Fig. 18 as a real process does not immediately mean that the vertex (b) of Fig. 47 indeed occurs as a real processes. Thus, we again put our emphasis on the fact that we include the vertex (b) of Fig. 47 into our diagram list because we have found it in our simulation.

## VI. A CONNECTION TO THE CONFINEMENT PROBLEM IN PARTICLE PHYSICS

So far, we have investigated the topological objects in nonrelativistic two component BECs in $2+1$ dimensions. At a glance, these seem to be very far from relativistic particle physics in $3+1$ dimensions. Nevertheless, the terminology (u, d, meson, baryon, and so on) and the description by Feynman diagrams borrowed from QCD are surprisingly fit for BECs. Although a precise connection between QCD and BECs is not clear at all, let us try to give some hints for understanding it along with the observations by Son and Stephanov in Ref. [8].

The key ingredient is duality. The vortices are particle-like topological defects in $2+1$ dimensions, and they are not elementary constituents of the original models. Nevertheless, it is known that a duality sometimes interchanges the defects and elementary constituents. A classic example is the duality between sine-Gordon solitons and fermions in the massive Thirring model in $1+1$ dimensions [40,41]. Another simple example relevant to this paper is particle-vortex duality between the $XY$ model and the Abelian-Higgs model in $2+1$ dimensions [42,43], which gives insights for understanding the fractional quantum Hall effect [44]. In the particle physics context, the dualities have been expected to be a powerful tool for us to understand nonperturbative dynamics in strongly coupled systems.

On the other hand, one of the most important unsolved problems in modern high-energy physics is the confinement of colors in QCD. The quarks and gluons are elementary

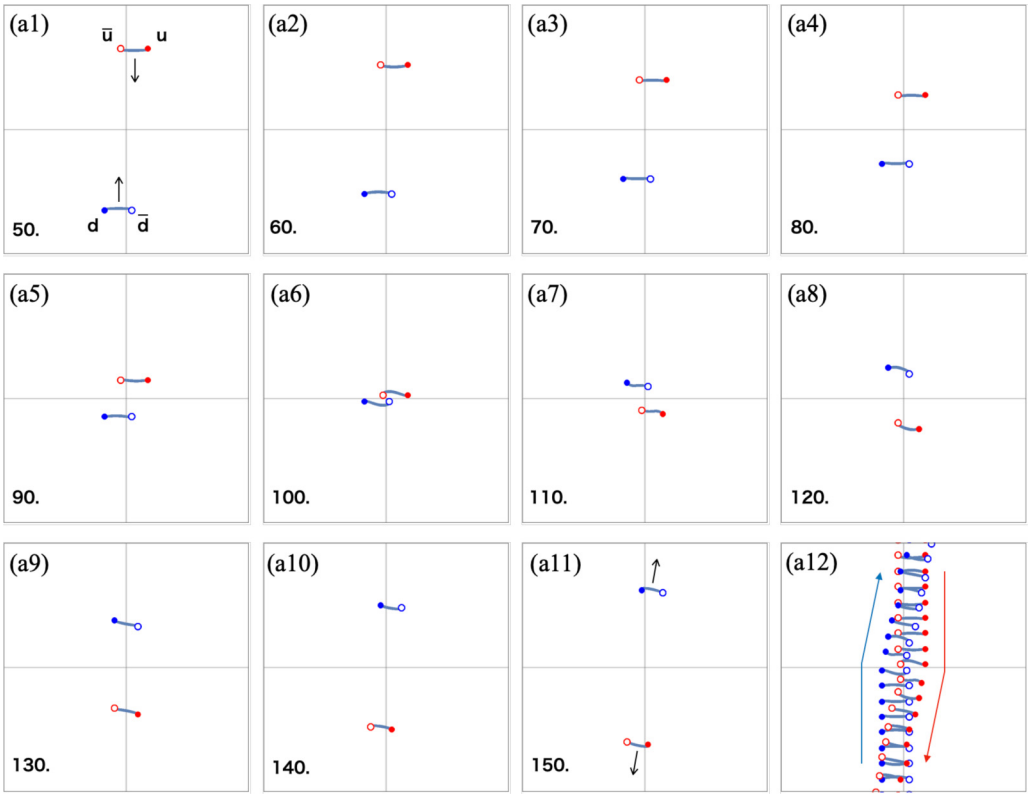


FIG. 37. The initial configuration is the same as that in Fig. 19 except for the fact that the lower meson is not $\bar{u}u$ but $\bar{d}d$. The plot region is $\tilde{x}_1 \in [-40, 40]$ (horizontal) and $\tilde{x}_2 \in [-40, 40]$ (vertical) and $\tilde{b} = 2.5$.

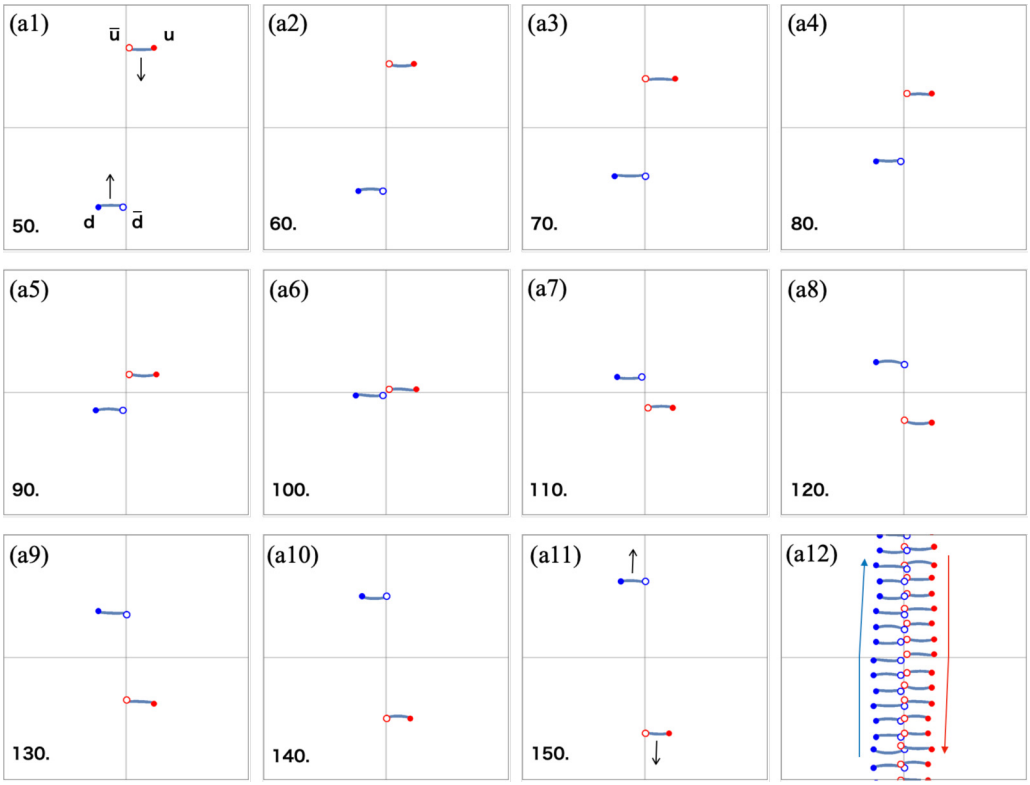


FIG. 38. The initial configuration is the same as that in Fig. 20 except for the fact that the lower meson is not ūu but d̄d. The plot region is $\tilde{x}_1 \in [-40, 40]$ (horizontal) and $\tilde{x}_2 \in [-40, 40]$ (vertical) and $\tilde{b} = 5$.

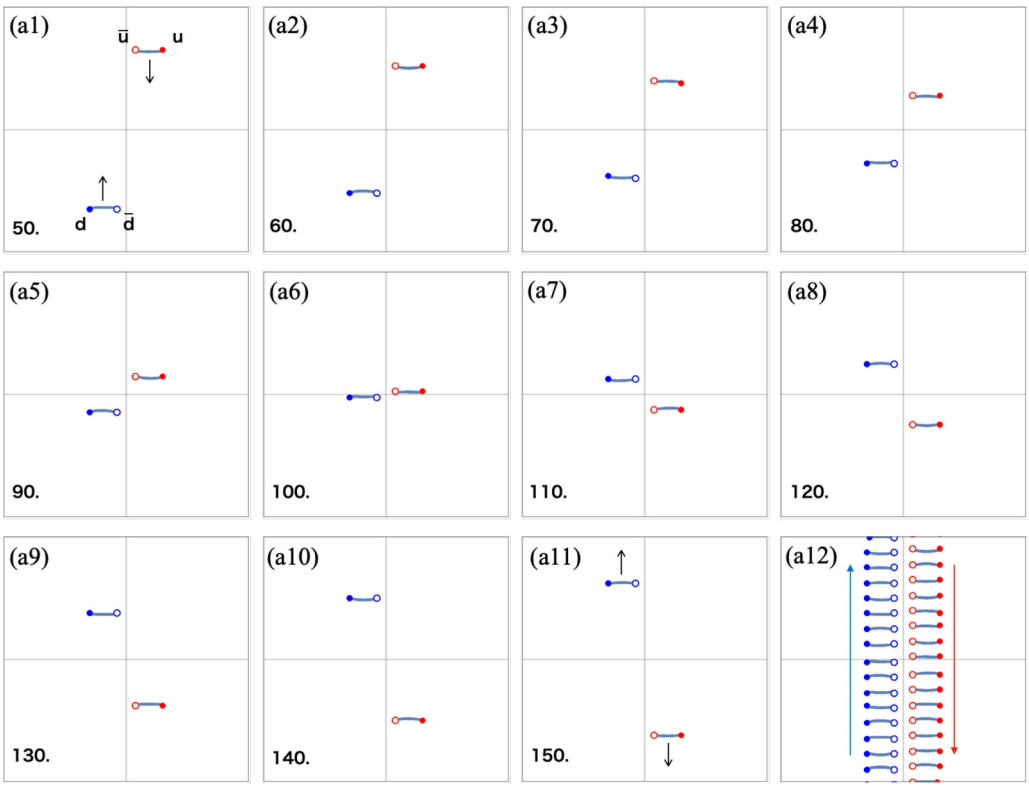


FIG. 39. The initial configuration is the same as that in Fig. 21 except for the fact that the lower meson is not ūu but d̄d. The plot region is $\tilde{x}_1 \in [-40, 40]$ (horizontal) and $\tilde{x}_2 \in [-40, 40]$ (vertical) and $\tilde{b} = 7.5$.

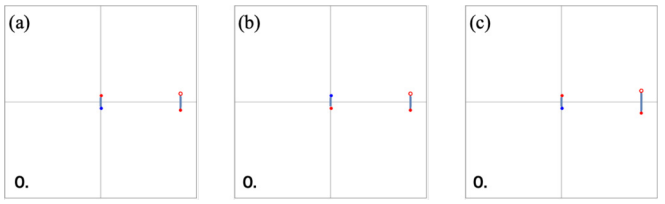


FIG. 40. The three initial configurations for a u meson and a baryon (ud) scattering. The region shown is $\tilde{x}_1 \in [-60, 60]$ (horizontal) and $\tilde{x}_2 \in [-60, 60]$ (vertical). The meson is placed at $(\tilde{x}_1, \tilde{x}_2) = (50, 0)$ and the target baryon is at the origin.

constituents of QCD, but we cannot observe them at low energy since they are strongly confined to form hadrons. Widely accepted picture of the confinement is that chromoelectric flux from a quark is squeezed to form a flux tube. Then interaction energy between (anti-)quarks is proportional to the separation distance, and they are confined. Though this picture of confinement is quite plausible, it is merely qualitative. Indeed, it is very difficult to prove analytically whether it occurs or not in real QCD. Then, instead of QCD, many studies have been done for QCD-like theories. An important milestone was achieved by Seiberg and Witten in supersymmetric $SU(2)$ Yang-Mills theory [45,46]. They analytically showed that condensation of the magnetic monopole indeed takes place at low energy.

Another important remark was made by Polyakov [47]. He considered a compact $U(1)$ gauge theory in $2+1$ dimensions which can be obtained as a low-energy effective theory of the Georgi-Glashow model with $SU(2)$ gauge field coupled to an adjoint scalar field $\phi_a$ $(a = 1, 2, 3)$. In the ground state, the adjoint scalar field develops a nonzero vacuum expectation value $\phi_a = (0, 0, v)$ and breaks $SU(2)$ down to its diagonal compact $U(1)$ subgroup. After integrating over all the massive fields, we are left with a free massless photon of the compact $U(1)$ group at low energy. Since the photon has only one polarization in three dimensions, it can be dualized to a periodic scalar field $\vartheta \in [0, 2\pi)$, a so-called dual photon, which is related to the original $U(1)$ gauge field $A_\mu$ by

$$F_{\mu\nu} = \frac{e^2}{4\pi}\varepsilon_{\mu\nu\rho}\partial^\rho\vartheta, \quad F_{\mu\nu} = \partial_\mu A_\nu - \partial_\nu A_\mu, \tag{26}$$

with $\mu, \nu = 0, 1, 2$ and $e$ is a $U(1)$ gauge coupling constant. Under the duality relation, electric charges in the original theory are interchanged by vortices in the dual theory as

$$\vartheta(z) = \sum_a q_a \mathrm{Im}\log(z - z_a) \tag{27}$$

with $z = x + iy$. Here $z_a$ are positions of vortices and $q_a = \pm 1$ are their charges. The dual photon is massless in perturbation theory but it attains mass by means of nonperturbative instanton ('t Hooft-Polyakov-type monopole) effects in the Georgi-Glashow model. In the weakly coupled region, the instantons interact with the Coulomb force and behave as a dilute plasma. Then the Debye screening effect gives a nonzero mass to the dual photon, which can be summarized

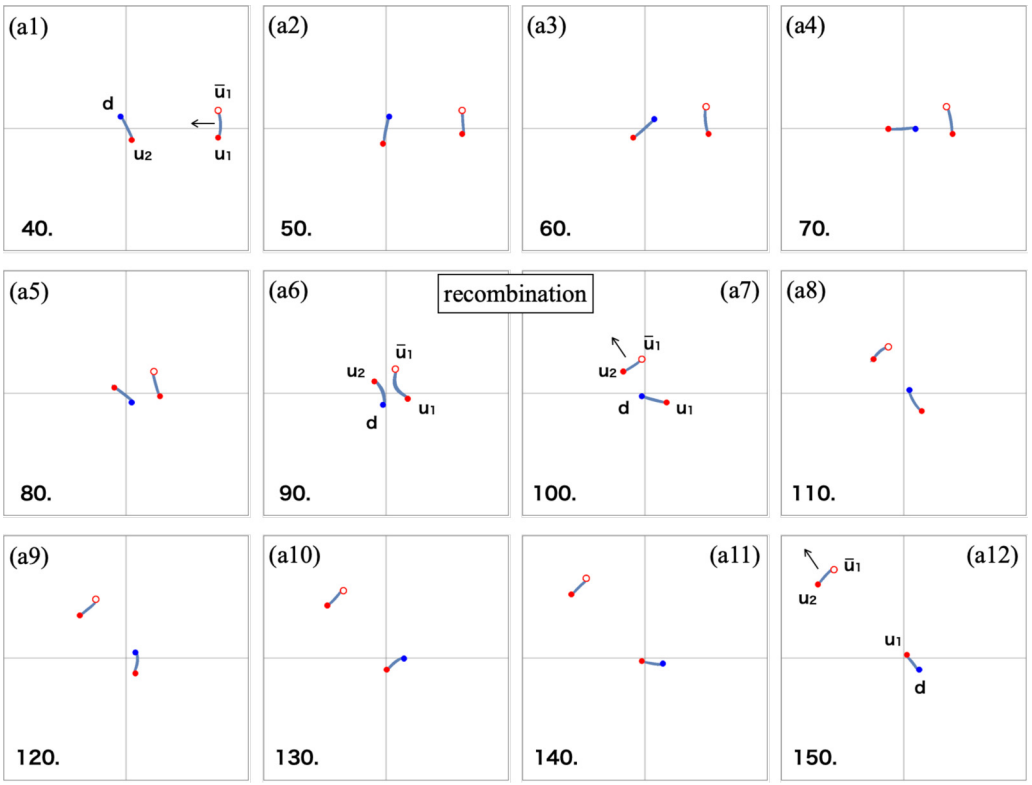


FIG. 41. The scattering of the meson $\bar{u}_1 u_1$ and the baryon $u_2 d$ with the initial configuration given in Fig. 40(a). The collision accompanies the recombination at about $\tilde{t} = 90$. The outgoing meson is $\bar{u}_1 u_2$ and the new baryon $u_1 d$ is left near the origin. We show the snapshots from $\tilde{t} = 40$ to 150 with interval $\delta\tilde{t} = 10$, and the plot region is $\tilde{x}_1 \in [-40, 40]$ (horizontal) and $\tilde{x}_2 \in [-40, 40]$ (vertical).

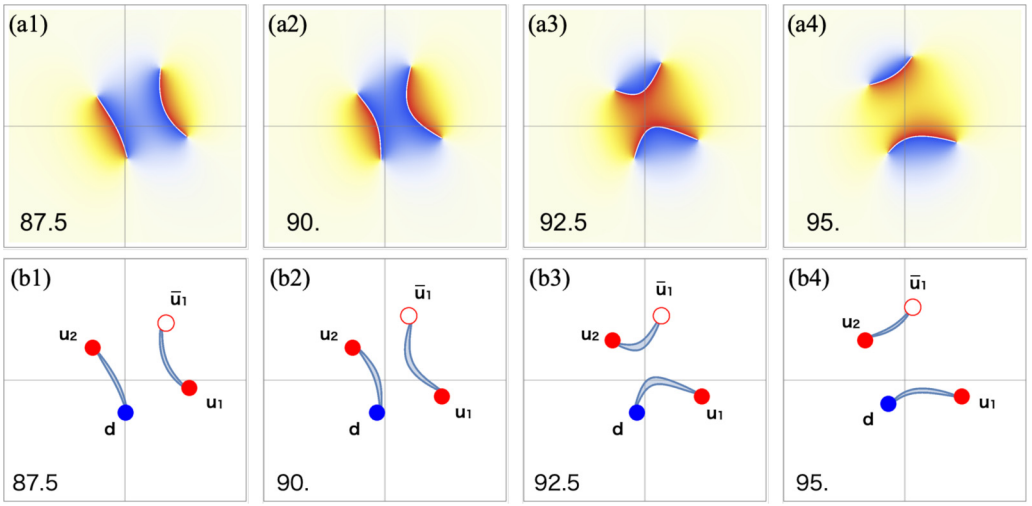


FIG. 42. Zoomed snapshots of Fig. 41 for the horizontal region $\tilde{x}_1 \in [-15, 15]$ and the vertical region $\tilde{x}_2 \in [-15, 15]$ at $\tilde{t} = 87.5, 90, 92.5, 95$ are shown.

in the following low-energy effective theory [47–50],

$$\mathcal{L}_{\text{eff}} = \frac{e^2}{32\pi^2}\partial_\mu\vartheta\partial^\mu\vartheta + c\xi\eta^3\cos\vartheta, \tag{28}$$

with $c$ being an undetermined parameter. The dimension full parameter $\eta$ is related to the mass $M_W$ of the massive gauge bosons as $\eta^3 = M_W^{7/2}/e$. The so-called monopole fugacity $\xi$ is exponentially small as $\xi = \exp(-\frac{2\pi M_W}{e^2}\epsilon)$, where $\epsilon$ is a function of the ratio of $M_W$ and the Higgs mass $M_\phi$, which is known to be of order one. From Eq. (28), the dual photon mass reads

$$M_\vartheta^2 = \frac{16\pi^2 c\eta^3\xi}{e^2}. \tag{29}$$

The nonperturbative instanton effects is responsible for another important phenomenon, the charge confinement.

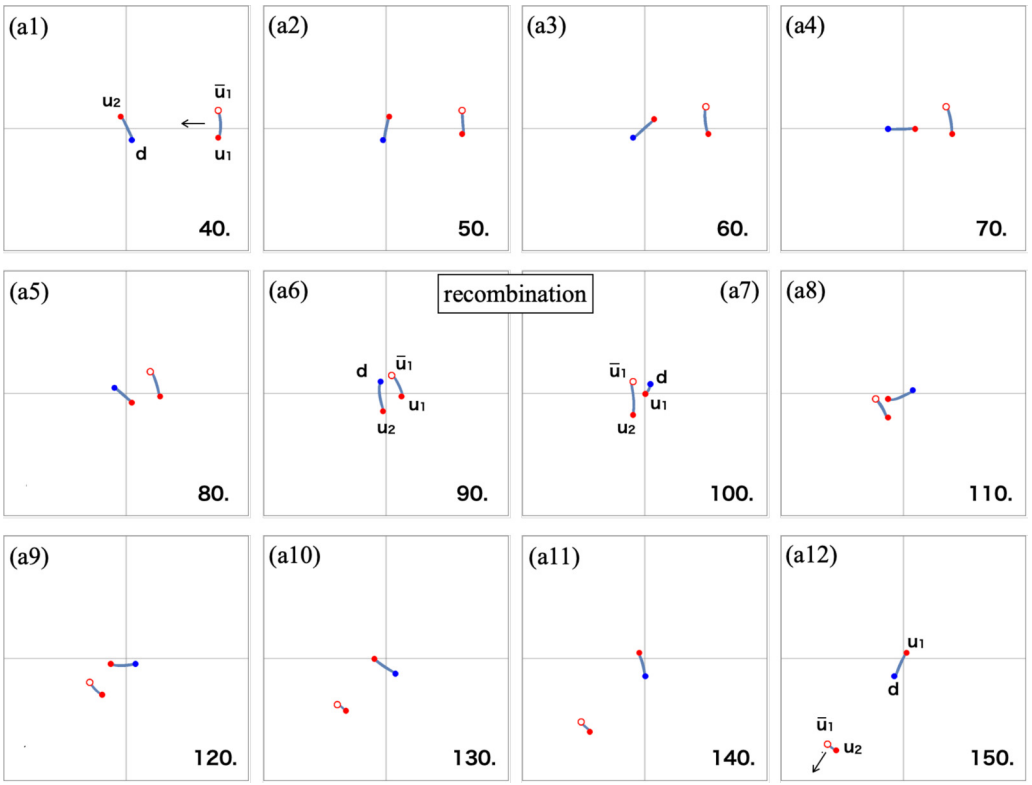


FIG. 43. The scattering of the meson $\bar{u}_1 u_1$ and the baryon $u_2 d$ with the initial configuration given in Fig. 40(b). The collision accompanies the recombination at about $\tilde{t} = 90$. The outgoing meson is $\bar{u}_1 u_2$ and the new baryon $u_1 d$ is left near the origin. We show the snapshots from $\tilde{t} = 40$ to 150 with interval $\delta\tilde{t} = 10$, and the plot region is $\tilde{x}_1 \in [-40, 40]$ (horizontal) and $\tilde{x}_2 \in [-40, 40]$ (vertical).

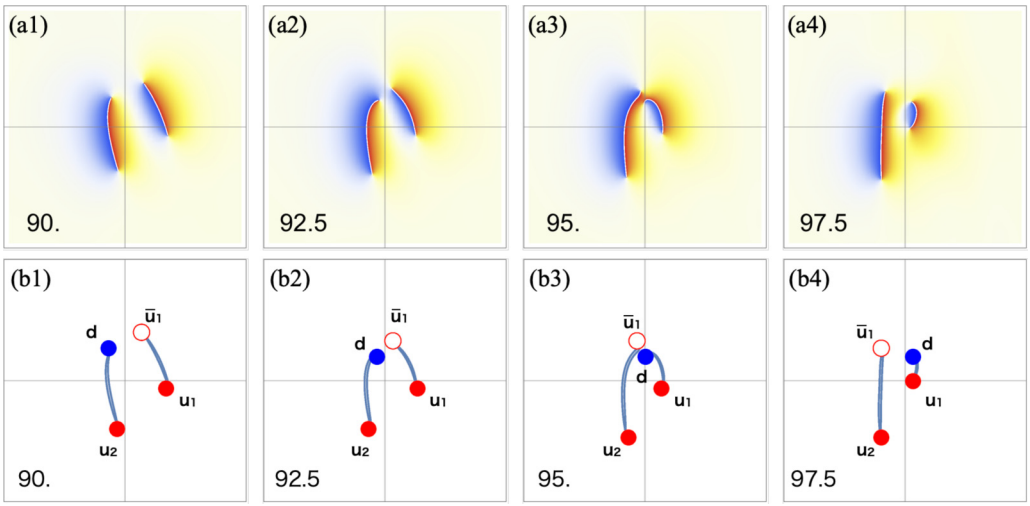


FIG. 44. Zoomed snapshots of Fig. 43 for the horizontal region $\tilde{x}_1 \in [-15, 15]$ and the vertical region $\tilde{x}_2 \in [-15, 15]$ at $\tilde{t} = 90, 92.5, 95, 97.5$ are shown.

Introducing a prove charge in the Georgi-Glashow model corresponds to putting a vortex in the dual theory as $\vartheta = \mathrm{Im} \log z = \theta$ ($z = re^{i\theta}$). When we go around the vortex, $\vartheta$ passes a potential peak once at $\theta = \pi$. Namely, a semi-infinite domain wall attaches at the vortex, and it corresponds to the confining string attached to the prove charge in the original picture. This is the standard understanding of confinement in the compact QED in $2 + 1$ dimensions.

Now we are in a position to observe a relation between the dual theory (28) and the Gross-Pitaevskii equations (1) of the 2 component BECs. The Lagrangian for Eq. (1) is given by

$$\mathcal{L}_{\mathrm{GP}} = \sum_i \left[ -\frac{i\hbar}{2}(\Psi_i \dot{\Psi}_i^* - \dot{\Psi}_i \Psi_i^*) - \frac{\hbar^2}{2m}|\nabla \Psi_i|^2 + \mu_i |\Psi_i|^2 - \frac{g_i}{2}|\Psi_i|^4 \right] - g_{12}|\Psi_1 \Psi_2|^2 - V_R, \tag{30}$$

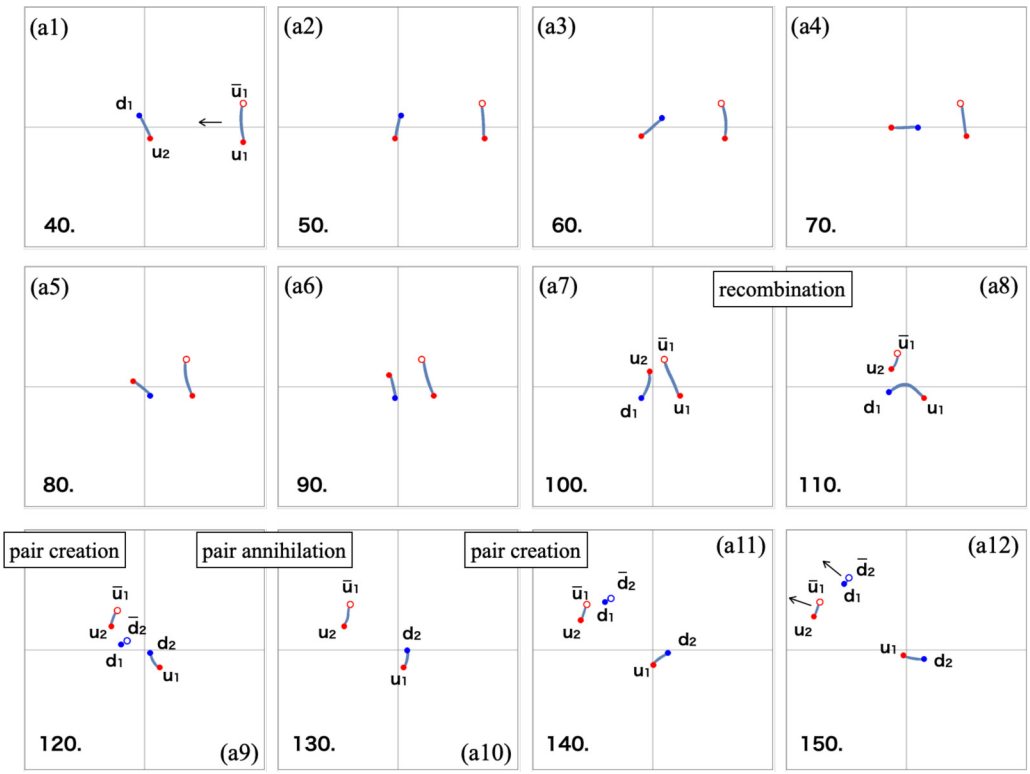


FIG. 45. The scattering of the meson $\bar{u}_1 u_1$ and the baryon $u_2 d$ with the initial configuration given in Fig. 40(c). The collision accompanies the recombination, pair creation, and pair annihilation. A new meson $\bar{d}_2 d_1$ is emitted, which we interpret as a vortical hadron jet. We show the snapshots from $\tilde{t} = 40$ to 150 with interval $\delta\tilde{t} = 10$, and the plot region is $\tilde{x}_1 \in [-40, 40]$ (horizontal) and $\tilde{x}_2 \in [-40, 40]$ (vertical).

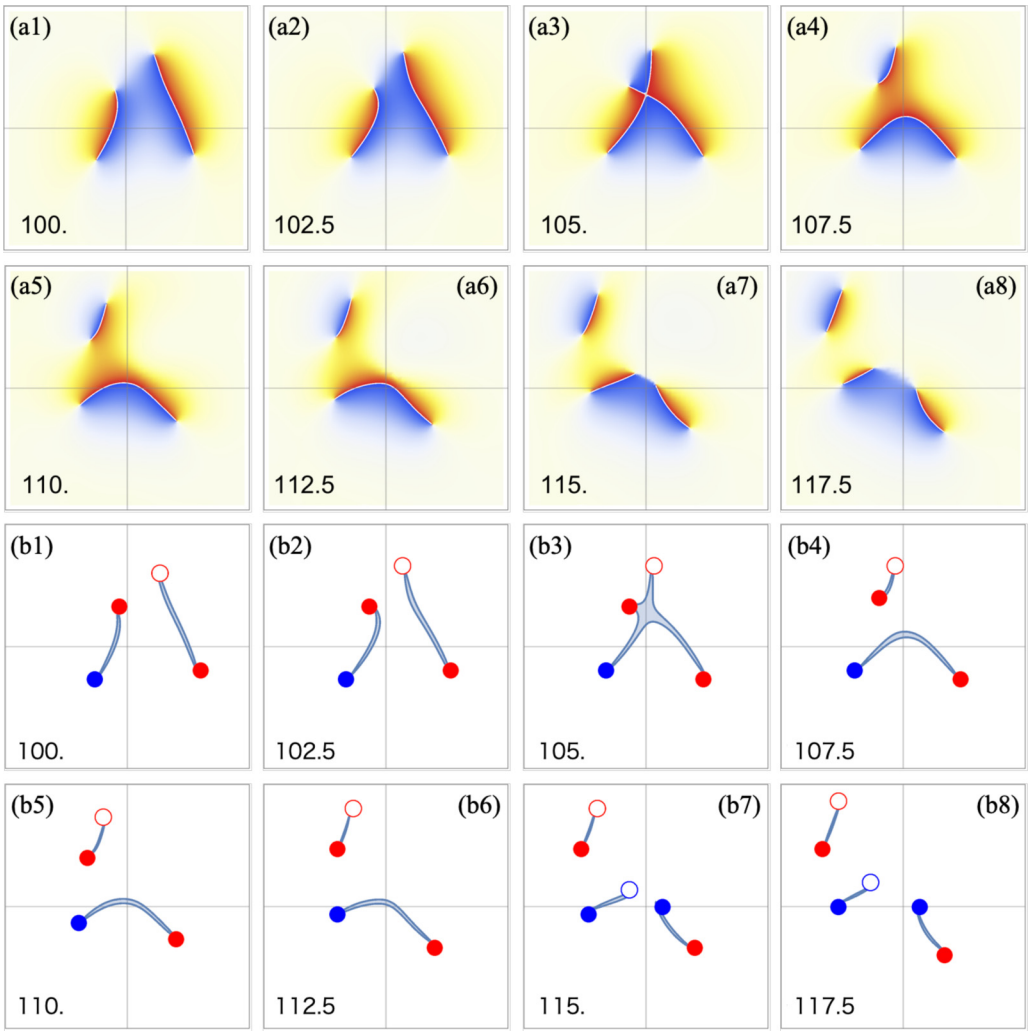


FIG. 46. Zoomed snapshots of Fig. 45 for the horizontal region $\tilde{x}_1 \in [-15, 15]$ and the vertical region $\tilde{x}_2 \in [-15, 15]$ from $\tilde{t} = 100$ to 117.5 with interval $\delta\tilde{t} = 2.5$ are shown.

with $V_{\rm R} = -\hbar\omega(\Psi_1\Psi_2^* + \Psi_1^*\Psi_2)$. Then we truncate this by substituting the expression of the condensates $\Psi_i = (v + r_i)e^{i\theta_i}$ into Eq. (30) and by integrating out the amplitude modes $r_i$ [8,16]:

$$\tilde{\mathcal{L}}_{\rm GP} = \tilde{\mathcal{L}}_S + \tilde{\mathcal{L}}_R, \tag{31}$$

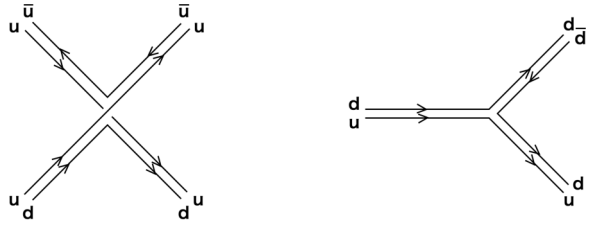


(a) (b)

FIG. 47. (a) Meson-meson-baryon-baryon vertex corresponding to the real process for Eq. (24). (b) Meson-meson-baryon vertex corresponds to the real process for Eq. (25).

with

$$\tilde{\mathcal{L}}_S = \frac{\hbar^2}{g + g_{12}}\dot{\theta}_S^2 - \frac{\hbar^2 v^2}{m}(\nabla\theta_S)^2, \tag{32}$$

$$\tilde{\mathcal{L}}_R = \frac{\hbar^2}{g - g_{12}}\dot{\theta}_R^2 - \frac{\hbar^2 v^2}{m}(\nabla\theta_R)^2 + 2\hbar\omega v^2\cos 2\theta_R, \tag{33}$$

where we have ignored constants and dealt with the Rabi term perturbatively. Here $\theta_S = (\theta_1 + \theta_2)/2$ is a phonon and $\theta_R = (\theta_1 - \theta_2)/2$ is known as the Leggett mode or phason. Note that the potential term in Eq. (33) is identical to $V_R$ given in Eq. (16). Now, we would like to identify $\mathcal{L}_{\rm eff}$ in Eq. (28) with $\tilde{\mathcal{L}}_R$ in Eq. (33). This can be achieved by making a correspondence as

$$\vartheta \Leftrightarrow 2\theta_R, \tag{34}$$

$$\frac{e^2}{8\pi^2} \Leftrightarrow \frac{\hbar^2}{g - g_{12}}, \tag{35}$$

$$c\xi\eta^3 \Leftrightarrow 2\hbar\omega v^2, \tag{36}$$

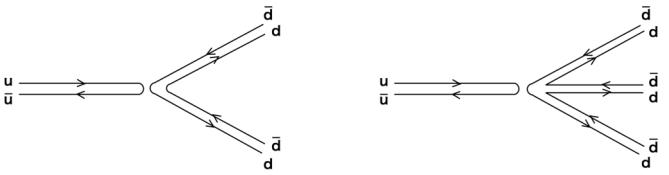


FIG. 48. Disconnected diagrams for ūu decay.

and we have rescaled the spatial coordinate as $\tilde{x}_i = \sqrt{\frac{m}{(g-g_{12})v^2}}\, x_i$ in Eq. (33).

The presence of the additional massless scalar field $\theta_S$ is a crucial difference between the Polyakov's dual theory (28) and the low-energy effective theory of the BECs in (31). We envisage a gauge theory whose gauge symmetry is broken like $U(1)_S \times SU(2) \to U(1)_S \times U(1)_R$ as an electric dual of the two-component BECs. Thanks to the additional $\theta_S$, we have two different species of the vortices, namely u- and d-vortices, and we can deal with not only the mesonic molecules but also the baryonic molecules unlike the original Polyakov's model. Furthermore, we emphasize that one of the nicest features of the two-component BECs is accessibility to the dynamical aspects of the confining phenomena as we have shown in this work.

Considering the duality pictures, we ask ourself again what the physical meaning of the Feynman diagrams is. Although we have no rigorous arguments, the classical diagrams of the u- and d-vortices would correspond to quantum Feynman diagrams of the elementary particles of the dual theory. For example, the classical one-loop diagram in Fig. 33 seems to be mapped onto the quantum one-loop diagram in the dual theory. If we could compute a quantum quantity from the dynamics of some classical topological defects in a very different theory, then it is interesting. We have no further observations pushing the idea forward, so we leave it as an open question at this moment.

Finally, as a possible clue for pinning down the connection between particle physics and two-component BECs, let us briefly mention the OZI rule [32–34], which is a phenomenological rule of QCD determined in the 1960s [35]. The OZI rule explains the narrow decay width of the vector meson. Kinematically, the decay $\phi(\bar{s}s) \to \pi^+(\bar{d}u) + \pi^0(\bar{d}d) + \pi^-(\bar{u}d)$ dominates the other decay process $\phi(\bar{s}s) \to K^+(\bar{s}u) + K^-(\bar{u}s)$ because the phase space of the former process is much larger than the latter. Nevertheless, the process $\phi \to 3\pi$ is highly suppressed relative to $\phi \to K^+K^-$. The OZI rule in QCD is a phenomenological postulation that diagrams with disconnected quark lines are suppressed relative to connected ones. It seems natural for us to ask whether a similar rule holds for hadronic molecules in two-component BECs or not. In order to answer this question, let us consider the decay of a ūu mesonic molecule and verify whether the diagrams given in Fig. 48 are observed. Throughout this work, we have met the decay diagrams of ūu three times. The first and the second ones are given in Fig. 18 (mmm3) and (mbb1), respectively. The third one is the leftmost diagram of Fig. 34. None of them are disconnected diagrams. Moreover, not only these three diagrams but also all the diagrams we encountered so far are connected diagrams. Thus, we have found an empirical rule that diagrams with disconnected vortex lines are highly suppressed relative to connected ones. Namely, the OZI rule seems to hold even in BECs. The OZI rule in QCD is explained as follows. Disconnected quark lines are indeed connected by internal gluon lines. High momentum transfer by the gluons makes the QCD coupling constant small, so that such channels are highly suppressed. Thus, the QCD OZI rules is a consequence of a quantum effect. On the other hand, the dynamics of vortical hadrons in BECs essentially obeys the classical GP equations. We expect that a counterpart of the gluon is the classical wave functions $\Psi_i$, and the classical OZI rule in BECs corresponds to the quantum OZI rule in QCD via a duality. As mentioned, we do not have a precise connection between QCD and BECs. This is another open question.

## VII. SUMMARY AND DISCUSSION

In this work, we have investigated the dynamics of the vortex molecules in two-component BECs by numerically solving the Gross-Pitaevskii equations (1). This paper is inline with previous works [8,14,16] focusing on the confinement property of fractional vortices by the SG solitons. While the dynamical property of an individual molecule, such as precession and disintegration, were figured out in Refs. [14,16], here we have studied the scattering and collision of molecules. Our numerical studies are twofold: the meson-meson scattering and the meson-baryon scattering.[2]

In Sec. III, we have dealt with the meson-meson scattering of the same species (ūu-ūu). First, we have demonstrated three simulations of the head-on collisions (zero impact parameter) by varying the incident angles, which are summarized in Fig. 14. We have found that the mesons collisions involve the vortical reaction given in Eq. (20). Namely, the constituent vortices swap their partners. We also showed that the recombination can be understood as a collision of the SG and anti-SG solitons, and the swapping is nothing but the pair annihilation and creation of the confining SG solitons as can be seen in Fig. 7. Of course, the details of the final states sensitively depend on the initial incident angle. The simulation with the initial relative angle $\pi$ happens to show the right-angle scattering of the two mesons, which is very common among relativistic topological solitons. On the other hand, the scattering with smaller angle $\pi/2$ exhibits a more complicated out-going state involving pair creation of a new

[2]For both the simulations, the nonrelativistic nature of the GP equations is crucial since it ensures that the molecule size is kept finite and constant even though the constituent vortices are pulled by the SG soliton. In relativistic models, this cannot happen because the molecules soon shrink. Especially, it is very difficult to prepare mesonic molecules which soon decay into radiation. The cost we have to pay is that both the precession speed of a baryonic molecule and the translation speed of a mesonic molecule are determined by the molecule size [16], but we can, nevertheless, make use of such dynamical properties (the precession of baryons and the translation of mesons) for planning scattering experiments of the mesons and baryons. Indeed, our numerical simulations provide quite rich and interesting results as we have described above.

meson and a subsequent pair annihilation of the original meson. In principle, there are a plethora of possible different scattering events depending on the model parameters, initial configurations, and so on. Clearly, solving numerically the GP equations for every possible parameter combination is not a good strategy. To avoid this inefficient approach and to get an efficient outlook, we developed a useful description by using Feynman diagrams. A fractional vortex corresponds to a line with an arrow toward the time direction, whereas an antifractional vortex is expressed by a line with an arrow opposite to the time direction. The elementary vertices found through the meson-meson scatterings with the aid of time reversal and the parity transformations are summarized in Fig. 18. These are the building blocks of the real scattering processes. We have also studied meson-meson scattering with nonzero impact parameters. It is found that the scattering angles depend on the impact parameter: The smaller the impact parameter, the larger the scattering angle. By increasing the impact parameter, the scattering angle is eventually reduced and crosses zero and becomes negative. Then, it asymptotically becomes zero as the impact parameter is taken to be infinity.

In Sec. IV, we have turned to studying the meson-meson scattering of the different species ($\bar{u}u$-$\bar{d}d$). We have repeated the numerical simulations similarly to those in Sec. III. The head-on collision with zero relative angle seems to be less interesting at a glance: The two mesons just pass through each other, see Fig. 24. However, we have found that the scattering of the two SG solitons occurs. They recoil, and the molecules interchange the SG solitons before and after the collision. However, studying the head-on collisions with the smaller relative angle is more interesting. We have found that the incoming u and d mesons are converted into the intermediate baryon and antibaryon pair during the collision. The intermediate baryons rotate and are then reformed back into the mesons at the second recombination. Forming the intermediate baryonic state results in the shift of the outgoing line from the ingoing one, see Fig. 32. As before, we have described the numerical simulations using Feynman diagrams and divided them into the elementary vertices. The newly found vertices are shown in Figs. 33. In addition, we also have put the new vertices in Figs. 34 and 35, corresponding to the disintegrations of the meson and baryon found in Refs. [14,16]. We also have studied the scatterings with nonzero impact parameters but the results are not so dramatic as those for the mesons of the same species.

In Sec. V, we have studied the meson-baryon scatterings ($\bar{u}u$ and ud). We have propagated the meson toward the baryon positioned at the origin. The observed variation in scattering arises from the difference of the relative angles of the two molecules at the collision point. We have examined two initial configurations (the molecules are initially parallel and antiparallel) given in the leftmost and the middle panels of Fig. 40. We have found that there are no qualitatively large differences between the two cases. In both cases, the meson and baryon swap their constituent u-vortices, and the new meson goes out while the new baryon stays at slightly shifted point from the original baryon point. Much more interesting things happen when we scatter a long meson to the baryon. The typical initial configuration is given in the rightmost panel of Fig. 40, and the scattering goes as shown in Fig. 45. The recombination takes place also in this case, so that a long and kink bend baryon is formed at first stage. However, such a long and bent molecule is unstable and soon disintegrates into a set of shorter mesons and baryons. As a result, the final state includes larger numbers of molecules than the prepared one. This somehow resembles what happens in real hadron collider experiments. When we collide two hadrons in a hadron collider with sufficiently large energy, thousands of hadrons come out as a hadron jet. Although our final state consists of only a few hadrons, we exaggeratedly call it a vortical hadron jet in the VHC experiment. It is surprising to us that the simple classical system (1) includes such rich phenomena somehow common to QCD which needs highly quantum regimes.

In Sec. VI, we have made supplementary comments in order to make a connection between QCD and BECs clearer. We have compared Polyakov's dual photon model in $2+1$ dimensions to the low-energy effective theory based on two-component BECs. We have seen the latter is an extension of the former, and so we expect the confinement of the u- and d-vortices studied here would shed some light on the confinement of elementary particles. An advantage of using BECs is that we can easily access dynamical aspects of the confinement which is in general difficult with QCD. As a related topic, we have also pointed out that a similar rule to the OZI rule in QCD seems to hold in BEC systems.

To close this paper, let us list what we have not done in this work. All the numerical analysis in this paper has been done under the condition of Eq. (2). Therefore, the u- and d-vortices have the same masses. The dynamics of the hadronic molecules for generic cases will be surely more complicated, but they might be more similar to QCD since the quarks have different masses in nature. Furthermore, we considered the model with two condensates. This is the reason why we have two different species, the u- and d-vortices. If we include three or more condensates, then we can consider hadrons consisting of more than two constituent vortices [23,24]. It would be especially interesting to study molecules such as a proton like molecule uud and a neutron like molecule udd to simulate situations closer to QCD. It might also be interesting to take into account the vortical hadrons at finite temperature and/or density. In QCD, there exist several phases such as quark gluon plasma and color superconducting phase. Exploring the phase diagram of the vortex matter in BEC would shed some light on the phase diagram of real QCD, see Ref. [51] for vortices in color superconductors in QCD.

Finally, we should in the future perform a comprehensive analysis of the connection between BECs and QCD. The results obtained in this work together with the previous studies of Refs. [8,16] support that these two very different theories are indeed related through dualities. However, as it currently stands this relationship is just an analogy, although it should be stated that the many notions of QCD can be accommodated by a theory describing a weakly interacting BEC. A key idea then for developing this connection further would be to develop our Feynman diagram approach used in this work, which was found to be very useful for describing the dynamics of vortices in BECs. In the context of quantum field theories, the use of Feynman diagrams is an aid to computation, since they allow one to compute scattering amplitudes. On the other

hand, it is unclear to us what computational benefit this approach has for BEC systems. In order to clarify this point, it is important to understand how these two models are connected via a duality, as well as the quantization of fractional vortices and their molecules in two component BECs. We focus on these points in the future.

## ACKNOWLEDGMENTS

The authors thank Matthew Edmonds for helpful comments. This work was supported by the Ministry of Education, Culture, Sports, Science (MEXT)-Supported Program for the Strategic Research Foundation at Private Universities "Topological Science" (Grant No. S1511006) and JSPS KAKENHI Grant No. 16H03984. The work of M.E. is also supported in part by JSPS Grant-in-Aid for Scientific Research KAKENHI Grant No. JP19K03839 and by MEXT KAKENHI Grant-in-Aid for Scientific Research on Innovative Areas "Discrete Geometric Analysis for Materials Design" No. JP17H06462 from the MEXT of Japan. The work of M.N. is also supported in part by JSPS KAKENHI Grant No. 18H01217 by a Grant-in-Aid for Scientific Research on Innovative Areas "Topological Materials Science" (KAKENHI Grant No. 15H05855) from MEXT of Japan.

[1] F. Dalfovo, S. Giorgini, L. P. Pitaevskii, and S. Stringari, Rev. Mod. Phys. **71**, 463 (1999).
[2] L. Pitaevskii and S. Stringari, *Bose-Einstein Condensation and Superfluidity* (Oxford University Press, Oxford, 2003),
[3] C. J. Pethick, and H. Smith, *Bose-Einstein Condensation in Dilute Gases* (Cambridge University Press, Cambridge, UK, 2008).
[4] A. L. Fetter, Rev. Mod. Phys. **81**, 647 (2009).
[5] D. V. Freilich, D. M. Bianchi, A. M. Kaufman, T. K. Langin, and D. S. Hall, Science **329**, 1182 (2010); S. Middelkamp, P. J. Torres, P. G. Kevrekidis, D. J. Frantzeskakis, R. Carretero-Gonzalez, P. Schmelcher, D. V. Freilich, and D. S. Hall, Phys. Rev. A **84**, 011605(R) (2011); R. Navarro, R. Carretero-Gonzalez, P. J. Torres, P. G. Kevrekidis, D. J. Frantzeskakis, M. W. Ray, E. Altuntas, and D. S. Hall, Phys. Rev. Lett. **110**, 225301 (2013).
[6] D. S. Hall, M. R. Matthews, J. R. Ensher, C. E. Wieman, and E. A. Cornell, Phys. Rev. Lett. **81**, 1539 (1998).
[7] M. R. Matthews, D. S. Hall, D. S. Jin, J. R. Ensher, C. E. Wieman, E. A. Cornell, F. Dalfovo, C. Minniti, and S. Stringari, Phys. Rev. Lett. **81**, 243 (1998); M. R. Matthews, B. P. Anderson, P. C. Haljan, D. S. Hall, M. J. Holland, J. E. Williams, C. E. Wieman, and E. A. Cornell, *ibid.* **83**, 3358 (1999); B. P. Anderson, P. C. Haljan, C. E. Wieman, and E. A. Cornell, *ibid.* **85**, 2857 (2000).
[8] D. T. Son and M. A. Stephanov, Phys. Rev. A **65**, 063621 (2002).
[9] J. J. Garcia-Ripoll, V. M. Perez-Garcia, and F. Sols, Phys. Rev. A **66**, 021602(R) (2002).
[10] K. Kasamatsu, M. Tsubota, and M. Ueda, Phys. Rev. Lett. **93**, 250406 (2004).
[11] K. Kasamatsu, M. Tsubota, and M. Ueda, Int. J. Mod. Phys. B **19**, 1835 (2005).
[12] M. Cipriani and M. Nitta, Phys. Rev. Lett. **111**, 170401 (2013).
[13] M. Nitta, M. Eto, and M. Cipriani, J. Low. Temp. Phys. **175**, 177 (2013).
[14] M. Tylutki, L. P. Pitaevskii, A. Recati, and S. Stringari, Phys. Rev. A **93**, 043623 (2016).
[15] L. Calderaro, A. L. Fetter, P. Massignan, P. Wittek, Phys. Rev. A **95**, 023605 (2017).
[16] M. Eto and M. Nitta, Phys. Rev. A **97**, 023613 (2018).
[17] M. Kobayashi, M. Eto, and M. Nitta, Phys. Rev. Lett. **123**, 075303 (2019).
[18] A. Usui and H. Takeuchi, Phys. Rev. A **91**, 063635 (2015).
[19] C. Qu, L. P. Pitaevskii, and S. Stringari, Phys. Rev. Lett. **116**, 160402 (2016).
[20] C. Qu, M. Tylutki, S. Stringari, and L. P. Pitaevskii, Phys. Rev. A **95**, 033614 (2017).
[21] K. Ihara and K. Kasamatsu, Phys. Rev. A **100**, 013630 (2019).
[22] P. Kuopanportti and J. A. M. Huhtamäki, and M. Möttönen, Phys. Rev. A **83**, 011603(R) (2011).
[23] M. Eto and M. Nitta, Phys. Rev. A **85**, 053645 (2012).
[24] M. Eto and M. Nitta, Europhys. Lett. **103**, 60006 (2013).
[25] M. Cipriani and M. Nitta, Phys. Rev. A **88**, 013634 (2013).
[26] D. S. Dantas, A. R. P. Lima, A. Chaves, C. A. S. Almeida, G. A. Farias, and M. V. Milošević, Phys. Rev. A **91**, 023630 (2015).
[27] N. V. Orlova, P. Kuopanportti, and M. V. Milošević, Phys. Rev. A **94**, 023617 (2016).
[28] S. H. Shinn and U. R. Fischer, Phys. Rev. A **98**, 053602 (2018).
[29] Y. Nambu, Phys. Rev. D **10**, 4262 (1974).
[30] G. 't Hooft, in *Proceedings of the E. P. S. International Conference on High Energy Physics*, edited by A. Zichichi (Editrice Compositori, Bologna, 1976).
[31] S. Mandelstam, Phys. Rept. **23**, 245 (1976).
[32] S. Okubo, Phys. Lett. **5**, 165 (1963).
[33] G. Zweig, An $SU_3$ model for strong interaction symmetry and its breaking, Version 1, Report No. CERN-TH-401, Particle Physics - Phenomenology (1964), p. 24.
[34] J. Iizuka, Prog. Theor. Phys. Suppl. **37**, 21 (1966).
[35] H. Fritzsch, *Murray Gell-Mann and the Physics of Quarks* (Springer, Berlin, 2018).
[36] M. Eto, K. Kasamatsu, M. Nitta, H. Takeuchi, and M. Tsubota, Phys. Rev. A **83**, 063603 (2011).
[37] See Supplemental Material at http://link.aps.org/supplemental/10.1103/PhysRevResearch.2.033373 for the movies of our numerical simulations.
[38] M. Kobayashi and M. Nitta, J. Low. Temp. Phys. **175**, 208 (2014).
[39] K. Kasamatsu, M. Eto, and M. Nitta, Phys. Rev. A **93**, 013615 (2016).
[40] S. R. Coleman, Phys. Rev. D **11**, 2088 (1975).
[41] S. Mandelstam, Phys. Rev. D **11**, 3026 (1975).

[42] M. E. Peskin, Ann. Phys. **113**, 122 (1978).
[43] C. Dasgupta and B. I. Halperin, Phys. Rev. Lett. **47**, 1556 (1981).
[44] D. H. Lee and M. P. A. Fisher, Phys. Rev. Lett. **63**, 903 (1989).
[45] N. Seiberg and E. Witten, Nucl. Phys. B **426**, 19, (1994); **430**, 485 (1994).
[46] N. Seiberg and E. Witten, Nucl. Phys. B **431**, 484 (1994).
[47] A. M. Polyakov, Nucl. Phys. B **120**, 429 (1977).
[48] I. I. Kogan and A. Kovner, in *At the Frontier of Particle Physics*, Vol. 4, edited by N. Shifman (World Scientific Publishing Co. Pte. Ltd, Singapore, 2002), pp. 2336–2407.
[49] D. Antonov and M. C. Diamantini, in *From Fields to Strings*, Vol. 1, edited by M. Shifman *et al.* (World Scientific Publishing, Singapore, 2005), pp. 188–265.
[50] M. Shifman and M. Unsal, Phys. Rev. D **78**, 065004 (2008).
[51] M. Eto, Y. Hirono, M. Nitta, and S. Yasui, PTEP **2014**, 012D01 (2014).